Commun. Comput. Phys.
doi: 10.4208/cicp.2009.09.049

Vol. **7**, No. 4, pp. 639-673
April 2010

Hyperbolic Moment Equations in Kinetic Gas Theory Based on Multi-Variate Pearson-IV-Distributions

Manuel Torrilhon*

Seminar for Applied Mathematics, ETH Zurich, Switzerland.

Received 9 March 2009; Accepted (in revised version) 27 July 2009

Communicated by Kun Xu

Available online 12 October 2009

Abstract. In this paper we develop a new closure theory for moment approximations in kinetic gas theory and derive hyperbolic moment equations for 13 fluid variables including stress and heat flux. Classical equations have either restricted hyperbolicity regions like Grad's moment equations or fail to include higher moments in a practical way like the entropy maximization approach. The new closure is based on Pearson-Type-IV distributions which reduce to Maxwellians in equilibrium, but allow anisotropies and skewness in non-equilibrium. The closure relations are essentially explicit and easy to evaluate. Hyperbolicity is shown numerically for a large range of values. Numerical solutions of Riemann problems demonstrate the capability of the new equations to handle strong non-equilibrium.

AMS subject classifications: 82B40, 35L40

Key words: Kinetic gas theory, moment approximations, hyperbolic partial differential equations.

1 Introduction

Many processes in gases are close to thermal equilibrium and can be described by fluid dynamic equations using the constitutive relations of Navier-Stokes and Fourier for stress and heat flux. In non-equilibrium processes these relations are no longer valid and the statistical description of kinetic gas theory has to be used. Moment approximations fill the gap between kinetic gas theory and fluid dynamics by deriving macroscopic partial differential equations that extend classical fluid dynamics to processes of strong non-equilibrium.

*Corresponding author. *Email address:* matorril@math.ethz.ch (M. Torrilhon)

Moment approximations have been introduced into kinetic theory by Grad [8,9] and refined from a thermodynamic point of view by Muller and Ruggeri, see the textbook [18]. In recent years there have been considerable progress in rigorously developing a practical, stable and accurate system of moment equations for non-equilibrium gases, see [10,26,27,30,31]. In the context of computational fluid dynamics moment equations have been considered, for example in [16,23,29].

Moment equations are partial differential equations for an extended set of fluid variables and consist of a non-dissipative first order flux operator and a dissipative part given by relaxation and, depending on the model, also diffusion. The flux part models the free flight of the particles, while the dissipation represents collisional interaction. One of the remaining issues in the development of moment equations is the hyperbolicity of the non-dissipative flux part, that is, real-valued characteristic speeds. Hyperbolicity allows to decouple the first order flux into advection equations reflecting the free flight transport. Non-hyperbolicity renders the first order moment system mathematically ill-posed and physically useless. Unfortunately, the classical moment equations of Grad are hyperbolic only relatively close to equilibrium [4,18,28].

Levermore in [15] focussed on hyperbolicity of moment equations and advocated the use of the maximum entropy distribution (see also [18]). Formally, the maximum entropy distribution provides closure relations that lead to globally hyperbolic moment equations. However, due to strong non-linearity it was so far not possible to derive explicit expressions for moment systems with more than 10 fields, i.e., higher than the second moment. Unfortunately, this so-called 10-moment-system is not capable to describe heat conduction and, hence, is of little practical use for gas processes. The works [12] by Junk and [13] by Junk & Unterreiter also indicates that higher systems based on the maximum entropy distribution might face severe mathematical problems.

This paper considers a Pearson-type-IV distribution for the distribution function of the particle velocities and shows that this gives globally hyperbolic moment equations. The use of a Pearson distribution comes as an ad-hoc assumption but is justified by the fact that it reduces to the Maxwellian distribution in equilibrium and allows for skewness and anisotropies in non-equilibrium to model stress and heat flux. The resulting moment equations consider 13 fields including stress tensor and heat flux. The closure relations are almost entirely explicit and easy to evaluate. Hyperbolicity is checked by numerical evaluation over a wide range of variable states. Additionally, Riemann problems are computed to demonstrate the ability of the new system to cope with strong non-equilibria.

Hyperbolicity is part of a larger group of properties desirable for a system of moment equations. This group contains for example Galilei-invariance, hyperbolicity, the existence of an entropy, and a positive realizable distribution function. The importance and relation of these properties is not clear and partly depends on the philosophy of the model. Ideally, a moment system would exhibit all these properties, but in general, it seems that they partly exclude each other. In this paper all systems of equations will be Galilei-invariant and hyperbolicity is the ultimate goal. To achieve this, we may com-

promise entropy and a realizable distribution. Indeed, the Pearson closure allows global hyperbolicity only without realizable distribution, while a realizable distribution gives a restricted hyperbolicity.

The rest of the paper is organized as follows. In the next section we introduce and discuss moment approximation in general together with the classical cases of Grad and maximum entropy. Section 3 introduces the Pearson-Type-IV distribution in one and three dimensions and computes its moments. Moment equations are then derived in Section 4. Valuable insights are taken from the 'toy-case' of a one-dimensional kinetic theory and afterwards used in the 3d-case. Section 5 discusses the results from different point of views and Section 6 presents numerical solutions in one space dimension. The paper ends with a conclusion and an appendix combining the details of the moment calculations for the Pearson distribution.

2 Moment approximations in kinetic gas theory

Kinetic gas theory describes the state of a gas at time t by means of the velocity distribution function in each space point $x\in\Omega\subset\mathbb{R}^D$. We have

$$f:\Omega\times\mathbb{R}^+\times\mathbb{R}^D\to\mathbb{R},\quad (\mathbf{x},t,\mathbf{c})\mapsto f(\mathbf{x},t,\mathbf{c}) \tag{2.1}$$

which makes the distribution function operating on a $2D+1$-dimensional domain in general. The relevant physical case is $D=3$, but we will also consider $D=1$ as model problem.

2.1 Equations

The distribution function follows the evolution equation

$$\partial_t f + c_i\partial_{x_i} f = S(f) \tag{2.2}$$

modeling free streaming of the particles by a transport operator and local particle interaction by $S(f)$. The interaction is typically modeled by Boltzmann's collision operator or a reduced variant, see for example the text books [5, 6]. In this paper $S(f)$ will play no role.

The theory of moment approximations introduces moments of the distribution function which in general are defined by

$$F_{i_1\cdots i_n}(x,t) = m\iiint_{\mathbb{R}^3} c_{i_1}\cdots c_{i_n} f(\mathbf{x},t,\mathbf{c})\,d\mathbf{c} \tag{2.3}$$

with particle mass m. The first moments F, F_i, and F_{kk} are the conservative variables of gas dynamics

$$\rho = m\int f(\mathbf{c})\,d\mathbf{c},\quad \rho v_i = m\int c_i f(\mathbf{c})\,d\mathbf{c},\quad \rho e+\frac{1}{2}\rho\mathbf{v}^2 = m\int\frac{1}{2}\mathbf{c}^2 f(\mathbf{c})\,d\mathbf{c}, \tag{2.4}$$

that is, the density, the momentum density and total energy density. We write the internal energy $e=\frac{3}{2}\theta$ with temperature θ in units of energy density.

The fundamental idea of moment approximations is to replace the high dimensional distribution function f by a finite set moments

$$f(\mathbf{x},t,\mathbf{c}),\mathbf{c}\in\mathbb{R}^3 \quad \leftrightarrow \quad \{F_{i_1\cdots i_n}(\mathbf{x},t)\}_{n=0,1,2,\cdots}. \tag{2.5}$$

The moments will still depend on space and time, but the additional dependency of f on the particle velocity $\mathbf{c}$ is substituted by the consideration of several moments. The working hypothesis is that a finite number of moments is sufficient to encode the details of f as a function of $\mathbf{c}$. Obviously, the motivation is that classical gas dynamics is very successful by describing the gas with less than 3 full moments.

It is easy to produce an evolution equation for the moments by applying the operation in (2.3) to the kinetic equation (2.2). We obtain

$$\partial_t F_{i_1\cdots i_n}+\partial_{x_k}F_{i_1\cdots i_n k}=P_{i_1\cdots i_n},\quad n=0,1,2,\cdots,$$

with the moment productions $P_{i_1\cdots i_n}$ which are integral of the interaction operator $S(f)$. In this paper we will only focus on the left hand side hence drop the production and consider the homogeneous moment system

$$\partial_t F_{i_1\cdots i_n}+\partial_{x_k}F_{i_1\cdots i_n k}=0,\quad n=0,1,2,\cdots. \tag{2.6}$$

Note, that this system essentially approximates the free flight equation

$$\partial_t f+c_i\partial_{x_i}f=0. \tag{2.7}$$

2.2 Closure problem

Every equation in the system of moment equations in (2.6) contains two moments, a lower one as variable in the time derivative and the next higher one as flux. With this structure the equations forms an infinite hierarchy, since every flux appears as variable in the next equation which itself has an even higher moment as flux.

If we cut the system for a certain finite number of moments we are exposed to a closure problems since the last flux needs to be related to lower moments in a reasonable fashion in order to have solvable closed equations.

2.2.1 Chapman-Enskog expansion

A classical approach is the Chapman-Enskog expansion, which is an asymptotic expansion for the non-equilibrium part of the distribution function. In equilibrium the distribution function has isotropic Gaussian shape and is given by

$$f_M(\mathbf{c};\rho,\mathbf{v},\theta)=\frac{\rho/m}{\sqrt{2\pi\theta}^3}\exp\left(-\frac{(\mathbf{c}-\mathbf{v})^2}{2\theta}\right), \tag{2.8}$$

the Maxwell distribution. It depends on the equilibrium variables density ρ, velocity $\mathbf{v}$, and temperature θ. Chapman and Enskog assumed an asymptotic expansion

$$f^{(\mathrm{CE})}(\mathbf{c};\rho,\mathbf{v},\theta) = f_M(\mathbf{c};\rho,\mathbf{v},\theta)\left(1+\varepsilon\varphi^{(1)}(\mathbf{c};\rho,\mathbf{v},\theta)+\varepsilon^2\varphi^{(2)}(\mathbf{c};\rho,\mathbf{v},\theta)+\mathcal{O}\left(\varepsilon^3\right)\right) \tag{2.9}$$

for the distribution function around equilibrium f_M. The smallness parameter ε is given by the Knudsen number, i.e., the ratio between men free path and observation scale. The first correction $\varphi^{(1)}$ leads to gradient expressions for stress and heat flux and reproduce the empirical laws of Navier-Stokes and Fourier, see [5,6]. However, the higher contributions lead to unstable equations, see [3].

2.2.2 General moment closure and hyperbolicity

In the moment approximation theory the closure is obtained from a model for the distribution function. A model of the distribution function has the form

$$f(\mathbf{x},t,\mathbf{c}) = f^{(\mathrm{model})}\left(\mathbf{c};\{\lambda_\alpha(\mathbf{x},t)\}_{|\alpha|=1,2,\cdots,N}\right) \tag{2.10}$$

such that f depends on space and time through parameters λ_α. Here we use multi-index notation $\lambda_\alpha = \lambda_{i_1\cdots i_{|\alpha|}}$. The number of parameters N represents the complexity of the model. We assume that the parameters can be computed from the first N moments after inserting $f^{(\mathrm{model})}$ into the definition of the moments (2.3) such that we have a one-to-one relation

$$\{F_\alpha\}_{|\alpha|=1,2,\cdots,N} \leftrightarrow \{\lambda_\alpha\}_{|\alpha|=1,2,\cdots,N} \tag{2.11}$$

between parameters and moments. If we now consider a moment hierarchy with N moments, the last flux of the moment system can be computed from integration of $f^{(\mathrm{model})}$ and in general depends on all lower moments in an algebraic way.

The final system (2.6) can be written

$$\partial_t u + \partial_{x_k} f_k(u) = 0, \tag{2.12}$$

where the variable vector $u \in V$ combines all moments in the phase space $V = \{F_\alpha\}_{|\alpha|=1,2,\cdots,N}$ and $f_k(u)$ are flux functions. Hyperbolicity is given by the following definition.

Definition 2.1 (Hyperbolicity)**.** *If for a phase state $u \in V$ and any unit vector $\mathbf{n} \in S^2$ the matrix*

$$A(\mathbf{n}) = n_k Df_k(u) \tag{2.13}$$

(based on the Jacobian Df_k) has only real eigenvalues, the system (2.12) *is hyperbolic in u.*

The eigenvalues are also called characteristic speeds and the region $H = \{u \in V \,|\, \text{hyperbolicity in } u\}$ is called region of hyperbolicity. Hyperbolicity is equivalent to the fact that for a fixed direction the system can be decomposed into advection equations, see for instance [14], with advection velocities that may depend non-linearly on u.

Hence, any moment system (2.6) should be hyperbolic, because the underlying physical phenomena is nothing but free flight (2.7), that is, a pure transport.

In this paper all hyperbolicity regions are computed numerically with help of the software package Mathematica. Typically, the direction $\mathbf{n}$ is chosen to be the x-direction. We then consider the scalar function

$$\psi(u) = \|\mathrm{Im}(\sigma(n_k Df_k(u)))\|_\infty, \tag{2.14}$$

where $\sigma(A)$ is the set of (complex) eigenvalues of the matrix A. The function $\psi(u)$ will be zero for $u \in H$. The border of H is plotted by producing a contour plot of ψ with the only contour $\psi = \varepsilon$ for very small ε, e.g., $\varepsilon = 10^{-3}$. Typically, the phase state for u is additionally projected onto a non-linear submanifold by appropriate scaling of the variables. In this way all hyperbolicity regions in this paper can be completely displayed in one or two dimensions even though the phase space is higher dimensional.

2.2.3 Grad's distribution function

When Grad considered moment equations in [8, 9] he solved the closure problem by assuming the general expression

$$f^{(\mathrm{Grad})}(\mathbf{x},t,\mathbf{c};\rho,\mathbf{v},\theta) = f_M(\mathbf{c};\rho,\mathbf{v},\theta)\left(1+\sum_{\alpha=1}^{N}\lambda_\alpha(\mathbf{x},t)\,\mathbf{c}_\alpha\right) \tag{2.15}$$

as model for the distribution function based on the Maxwellian distribution. Here, we additionally used the multi-index notation for $\mathbf{c}_\alpha = c_{i_1}\cdots c_{i_{|\alpha|}}$ to simplify the presentation. The Maxwellian in (2.15) depends on the local values of density, velocity and temperature. The ansatz (2.15) represents a partial sum of a Hermite series for the distribution function written in monomials $\mathbf{c}_\alpha$. From a functional analytical point of view we assume that for smooth f this partial sum yields a reasonable approximation. With this interpretation Grad's distribution function is not restricted to be close to equilibrium. Still, for λ_α small in some sense (2.15) can be viewed as perturbation of a Maxwellian.

The parameters λ_α are related to the moments after integrating $f^{(\mathrm{Grad})}$. The resulting system is linear and in general we obtain an explicit one-to-one relation for the first N moments and the parameters. The flux F_{Nk} of the last moment equation can now be computed from integration of (2.15).

2.2.4 Non-hyperbolicity of Grad's approach

The first interesting case beyond equilibrium considered by Grad uses the 13 fields of the moments F, F_i, F_{ij}, and F_{ikk}. This corresponds to density, velocity, temperature, stress deviator, and heat flux. For details of the derivation see [8, 9, 18]. The final system is known as Grad's 13-moment-equations.

In a process that varies only in one space dimension (say x-direction) we consider the fields density ρ, velocity v_x, pressure p, normal stress σ, and heat flux q_x. The general

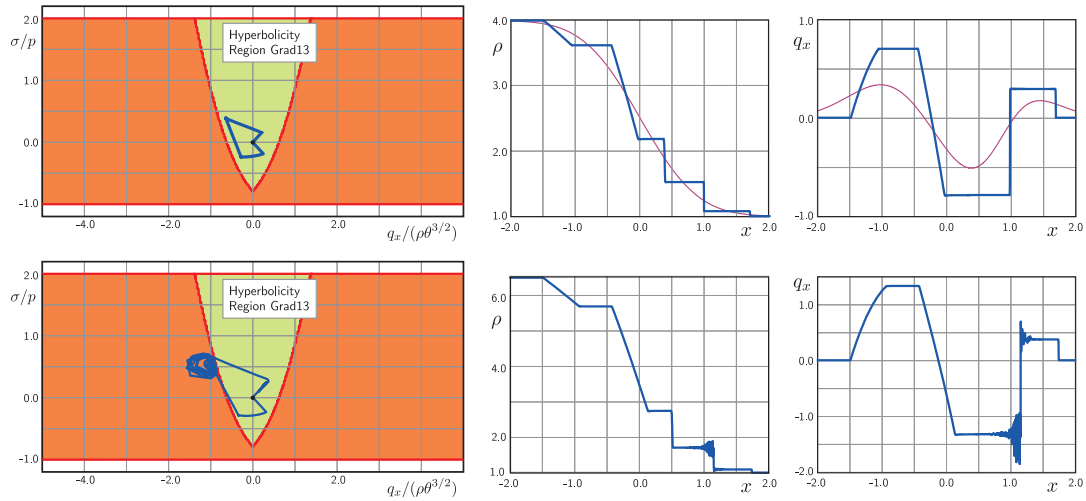

Figure 1: Hyperbolicity region (left: green area) and two different Riemann problems for Grad's 13 moment equations. For density ratio larger than 5 the ellipticity of the equations lead to oscillations and break-down of the computation.

system (2.6) reduces to 5 partial differential equations in space and time[†]. It turns out that this system is not globally hyperbolic. There are physical values of the fields such that complex eigenvalues arise from the flux function. The region of hyperbolicity can be displayed in the plane opened by the dimensionless normal stress σ/p and the dimensionless heat flux $q_x/(\rho\theta^{3/2})$. The left hand side of Fig. 1 shows this plane with the region of hyperbolicity marked as green area. The dot in the middle marks equilibrium $\sigma=0$ and $q_x=0$. Hyperbolicity is given for not too large heat fluxes and not too small stress values. Because the second moment F_{ij} is positive definite the normal stress can only take values $\sigma/p\in[-1,2]$. For large values of the heat flux and for very small values of σ/p hyperbolicity is lost.

To demonstrate the influence of this lack of hyperbolicity we compute a standard Riemann problem, see also Section 6 and [28] for details. The result for density and heat flux is displayed on the right hand side of Fig. 1 for two different initial conditions. On the top the initial density and pressure ratio is 4, on the bottom the ratio is 6.5. Note that the result looks very different to classical gas dynamics. The reason is that the Grad system approximates the free flight equation (2.7). In the top of the figure the analytical result for (2.7) is shown for comparison. Details of the analytical results of the collision-less Boltzmann equation for Riemann problems can be found, e.g., in [2]. The solutions of Grad's equations are also shown in the $(q_x/(\rho\theta^{3/2}),\sigma/p)$-plane as a closed curve parametrized by the space variable x.

For stronger initial density and pressure ratios the heat flux increases and the solution leaves the region of hyperbolicity. Complex eigenvalues lead to strong oscillations which

[†]The system can be produced from (4.27) below when using $m_{xxx}=\frac{6}{5}q_x$ and $R_{xx}=5\rho\theta^2+7\theta\sigma$.

grow and lead to a break down of the computation due to negative densities. This behavior severely limits the application range of Grad's equations. It can not be improved by considering more moments [2, 4]. The precise mathematical reason for the failure remains unclear. Most likely, the fact that the distribution function (2.15) becomes negative causes trouble. For the same reason the definition of an entropy by $f\ln f$ fails for Grad's equations.

Recently, Chapman-Enskog expansion have been used in [24, 25] to obtain proper scalings of the moments which yields a natural closure condition for moment system. This so-called order-of-magnitude approach yields moment equations which are linearly stable, and very similar to Grad's moment equations. Even though a rigorous investigation is open, due to the similarity these systems can be expected to exhibit comparable deficiencies in terms of hyperbolicity.

2.2.5 Maximum entropy distribution function

In [15, 18] it has been shown that when maximizing the kinetic entropy $f\ln f$ under the constraints of N given moments the distribution function has the form

$$f^{(\mathrm{ME})}(\mathbf{x},t,\mathbf{c}) = \exp\left(1+\sum_{\alpha=1}^{N}\lambda_\alpha(\mathbf{x},t)\,\mathbf{c}_\alpha\right), \tag{2.16}$$

where the λ_α's take the role of Lagrange multipliers in the maximization. It can be formally shown that this model induces hyperbolic moment equations when used to compute the last flux [15]. However, except when $N=2$ the mapping between the parameters and the moments

$$\{F_\alpha\}_{|\alpha|=1,2,\cdots,N} \leftrightarrow \{\lambda_\alpha\}_{|\alpha|=1,2,\cdots,N} \tag{2.17}$$

is highly non-linear and can not be solved analytically. Furthermore, it has been shown in [12] for a model system and in [13] for general systems that the domain of definition for a realizable distribution in (2.16) is non-convex and the fluxes of the moment equations become singular arbitrarily close to equilibrium. Hence, beyond $N=2$, the maximized-entropy-distribution $f^{(\mathrm{ME})}$ was never used in practical computations. Various modifications of (2.16) have been proposed to remedy this drawback, for example in [1], but they were not successful, so far.

2.2.6 Discontinuous models

Obviously, there are many ways to construct a model to approximate the distribution function. One further popular method is to use discontinuous or piece-wise Maxwell distributions with different variances and translations. In [17] shock waves have been computed based on the superposition of two Maxwellian distributions. Discontinuous distributions have been used [32] for sound dispersion and in [7] for shear flows. Typically, these models are defined for a concrete geometry or process and lack generality. For these models hyperbolicity have not been studied.

3 Pearson-Type-IV distribution function

3.1 One-dimensional case

The Pearson distributions type I-XII for a one-dimensional variable have been introduced in a series of papers [20–22]. For our purpose only type IV is relevant. A good introduction can be found in [11]. Pearson describes a distribution with four real parameters: a translation λ, a scale $a>0$, a skewness ν, and a shape factor $\bar{m}>0$[‡]. The function is given by

$$f^{(\mathrm{P1})}(c;\lambda,a,\bar{m},\nu)=\frac{1}{ak}\frac{\exp\left(-\nu\arctan\left(\frac{c-\lambda}{a}\right)\right)}{\left(1+\left(\frac{c-\lambda}{a}\right)^2\right)^{\bar{m}}} \tag{3.1}$$

with normalization constant k. Explicit expressions for the normalization constant can be found in [19,20].

We denote the first moment by v (velocity in our context) and find

$$v=\int_{-\infty}^{\infty} c f^{(\mathrm{P1})}(c;\lambda,a,\bar{m},\nu)\,dc=\lambda-\frac{a\nu}{2(\bar{m}-1)} \tag{3.2}$$

after suitable integration which is outlined in Appendix A.1.1. In one-dimensional calculations it becomes useful to define

$$r=2(\bar{m}-1) \tag{3.3}$$

as abbreviation. General moments of the distribution are defined by

$$\mu_n(\lambda,a,\bar{m},\nu)=\int_{-\infty}^{\infty}(c-v)^n f^{(\mathrm{P1})}(c;\lambda,a,\bar{m},\nu)\,dc \tag{3.4}$$

for $n>1$. In the Appendix A.1.2 it is shown that the recursion

$$\mu_n=\frac{a(n-1)}{r-(n-1)}\left(\left(1+\left(\frac{\nu}{r}\right)^2\right)a\mu_{n-2}-\frac{2\nu}{r}\mu_{n-1}\right) \tag{3.5}$$

holds for the moments with starting relations $\mu_0=1$ and $\mu_1=0$.

If we define the temperature and the reduced third and fourth moment by

$$\theta=\mu_2,\quad Q=\frac{\mu_3}{\mu_2^{3/2}},\quad D=\frac{\mu_4}{\mu_2^2}, \tag{3.6}$$

we can compute the parameters of the distribution from the first four moments with the simple expressions

$$\begin{aligned} r&=\frac{6(D-Q^2-1)}{2D-3Q^2-6},\quad \nu=-\frac{r(r-2)Q}{\sqrt{16(r-1)-Q^2(r-2)^2}},\\ a&=\sqrt{\theta}\sqrt{r-1-\frac{1}{16}Q^2(r-2)^2},\quad \lambda=v-\frac{1}{4}(r-2)Q\sqrt{\theta}, \end{aligned} \tag{3.7}$$

[‡]The standard notation for the shape factor is m, which we write $\bar{m}$ in order not to confuse it with the particle mass.

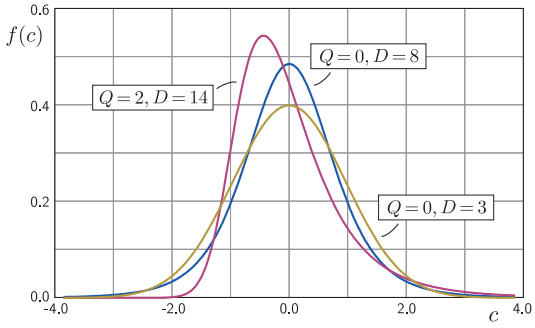

Figure 2: Pearson Type IV distributions with unit temperature, zero velocity and different third and fourth moment, Q and D. In equilibrium, $Q=0, D=3$, the distribution becomes Gaussian.

which can also be found, e.g., in [19]. Because ν and a need to be real and $r>-2$ ($\bar{m}>0$), we find the realizability condition

$$D \geq D^{(\text{crit})} = \frac{48+39Q^2+6\sqrt{(4+Q^2)^3}}{32-Q^2}, \quad |Q|<\sqrt{32} \tag{3.8}$$

for Pearson IV when given the first four moments.

It is very important to note that for $Q=0$ we have $\nu=0$ and $a=\sqrt{(2\bar{m}-3)\theta}$ and it is easy to see that

$$\lim_{m\to\infty} f^{(\text{P1})}(c;\lambda,a,\bar{m},0) = \lim_{m\to\infty} \frac{1}{ak} \frac{1}{\left(1+\left(\frac{c-\lambda}{a}\right)^2\right)^{\bar{m}}} = \frac{1}{\sqrt{2\pi\theta}} \exp\left(-\frac{(c-\lambda)^2}{2\theta}\right), \tag{3.9}$$

hence, the Pearson distribution reduces to a Gaussian if the shape factor $\bar{m}$ goes to infinity and $Q=0$. Only for $\bar{m}\to\infty$ the distribution has exponential decay, while for $\bar{m}<\infty$ it is heavy-tailed.

Fig. 2 shows some examples of Pearson IV distributions for different values of the reduced third and fourth moment. All curves have zero velocity and unit temperature.

3.2 Three-dimensional case

3.2.1 Definition

The gas particle velocity $\mathbf{c}\in\mathbb{R}^3$ is a vector in 3-space. Hence, the Pearson IV distribution introduced in the previous section needs to be extended to the three-dimensional case. In this setting the translation becomes a vector $\boldsymbol{\lambda}\in\mathbb{R}^3$, and the scale a symmetric positive definite 3×3-matrix $\mathbf{A}\in\mathbb{R}^{3\times3}$. The skewness parameter ν is supplemented by a direction of the skewness $\mathbf{n}\in S^2$. The shape parameter $\bar{m}>0$ remains the same. In this way the distribution is described by 14 real parameters.

The distribution function is given by

$$f^{(\mathrm{P3})}(\mathbf{c};\boldsymbol{\lambda},\mathbf{A},\bar{m},\nu,\mathbf{n}) = \frac{1}{\det(\mathbf{A})K}\frac{\exp\left(-\nu\arctan\left(\mathbf{n}^T\mathbf{A}^{-1}(\mathbf{c}-\boldsymbol{\lambda})\right)\right)}{\left(1+(\mathbf{c}-\boldsymbol{\lambda})^T\mathbf{A}^{-2}(\mathbf{c}-\boldsymbol{\lambda})\right)^{\bar{m}}} \tag{3.10}$$

with normalization constant

$$K = \frac{1}{\det(\mathbf{A})}\iiint_{\mathbb{R}^3}\frac{\exp\left(-\nu\arctan\left(\mathbf{n}^T\mathbf{A}^{-1}(\mathbf{c}-\boldsymbol{\lambda})\right)\right)}{\left(1+(\mathbf{c}-\boldsymbol{\lambda})^T\mathbf{A}^{-2}(\mathbf{c}-\boldsymbol{\lambda})\right)^{\bar{m}}}d\mathbf{c}. \tag{3.11}$$

This constant does only depend on $\bar{m}$ and ν which is shown in Appendix A.2.1. There, it is also demonstrate that the three-dimensional integral factorizes into integrals over 1D Pearson distributions. This procedure is key to the computation of moments of the distribution in three dimensions and leads to the fact that all 3D-moments are analytically computable with expressions very similar to the one-dimensional case.

3.2.2 Velocity and general moments

The velocity can be expressed by

$$\mathbf{v} = \iiint_{\mathbb{R}^3}\mathbf{c}\,f^{(\mathrm{P3})}(\mathbf{c};\boldsymbol{\lambda},\mathbf{A},\bar{m},\nu,\mathbf{n})\,d\mathbf{c} = \boldsymbol{\lambda}+\mathbf{A}\iiint_{\mathbb{R}^3}\tilde{\mathbf{c}}\,f^{(\mathrm{P3})}(\tilde{\mathbf{c}};\mathbf{0},\mathbf{I},\bar{m},\nu,\mathbf{n})\,d\tilde{\mathbf{c}} \tag{3.12}$$

with the transformation of $\mathbf{c}$ as in Appendix A.2.1. From tensor representation theory the remaining integral must have the form

$$\iiint_{\mathbb{R}^3}\tilde{\mathbf{c}}\,f^{(\mathrm{P3})}(\tilde{\mathbf{c}};\mathbf{0},\mathbf{I},\bar{m},\nu,\mathbf{n})\,d\tilde{\mathbf{c}} = \alpha\,\mathbf{n}, \tag{3.13}$$

since $\mathbf{n}$ is the only available vector in the integrand. The scalar α follows from scalar multiplication with $\mathbf{n}$ which transforms the vectorial integral into a scalar one and reads $\alpha = -\frac{\nu}{2(\bar{m}-2)}$ (see Appendix A.2.1) such that we find

$$\mathbf{v} = \boldsymbol{\lambda} - \frac{\nu}{2(\bar{m}-2)}\mathbf{A}\,\mathbf{n} \tag{3.14}$$

for the velocity. Here, in the three-dimensional case it is useful to define

$$r = 2(\bar{m}-2) \tag{3.15}$$

instead of (3.3). With this the similarity of the moment expressions of the one- and three-dimensional case becomes clear. We will use $r^{(1\mathrm{D})}$ and $r^{(3\mathrm{D})}$ in the rare cases where confusion is possible.

General moments of the Pearson distribution are defined by

$$M_{i_1\cdots i_n} = \iiint_{\mathbb{R}^3}(c_{i_1}-v_{i_1})\cdots(c_{i_n}-v_{i_n})\,f^{(\mathrm{P3})}(\mathbf{c};\boldsymbol{\lambda},\mathbf{A},\bar{m},\nu,\mathbf{n})\,d\mathbf{c}, \tag{3.16}$$

which are tensorial quantities of degree n. To compute the moments this integral will be transformed according to

$$\begin{aligned} M_{i_1\cdots i_n} &= \iiint_{\mathbb{R}^3} (A_{i_1 j_1}\tilde{c}_{j_1}+\lambda_{i_1}-v_{i_1})\cdots(A_{i_n j_n}\tilde{c}_{j_n}+\lambda_{i_n}-v_{i_n}) f^{(\mathrm{P3})}(\tilde{\mathbf{c}};0,\mathbf{I},\bar{m},\nu,\mathbf{n})\,d\tilde{\mathbf{c}} \\ &= A_{i_1 j_1}\cdots A_{i_n j_n}\iiint_{\mathbb{R}^3}(\tilde{c}_{j_1}-\tilde{v}_{j_1})\cdots(\tilde{c}_{j_n}-\tilde{v}_{j_n}) f^{(\mathrm{P3})}(\tilde{\mathbf{c}};0,\mathbf{I},\bar{m},\nu,\mathbf{n})\,d\tilde{\mathbf{c}} \end{aligned} \tag{3.17}$$

with the abbreviation

$$\tilde{\mathbf{v}} = -\frac{\nu}{r}\mathbf{n}. \tag{3.18}$$

A general expression for the remaining integral has not been found. To evaluate it for specific cases below it is useful to know the integral

$$\tilde{\mu}_n^{p,q} = \frac{1}{K}\iiint_{\mathbb{R}^3}(\tilde{c}_1-\tilde{v}_1)^n \tilde{c}_2^p \tilde{c}_3^q \frac{\exp\left(-\nu\arctan(\tilde{c}_1)\right)}{\left(1+\tilde{c}_1^2+\tilde{c}_2^2+\tilde{c}_3^2\right)^{\bar{m}}} d\tilde{\mathbf{c}}, \tag{3.19}$$

which can be viewed as a generalization of the one-dimensional moments μ_n. In the formula p and q are even otherwise $\tilde{\mu}_n^{p,q}=0$. Additionally, we have the symmetry $\tilde{\mu}_n^{p,q}=\tilde{\mu}_n^{q,p}$. In Appendix A.2.2 it is shown that $\tilde{\mu}_n^{p,q}$ satisfies a recursion similar to the one-dimensional case. It reads

$$\tilde{\mu}_n^{p,q} = \frac{1}{r-(p+q)-(n-1)}\left((n-1)\left(1+\left(\frac{\nu}{r}\right)^2\right)\mu_{n-2}^{p,q} - (2(n-1)+p+q)\frac{\nu}{r}\mu_{n-1}^{p,q}\right) \tag{3.20}$$

with starting condition

$$\tilde{\mu}_0^{p,q} = (p-1)!!(q-1)!!\prod_{k=1}^{\frac{p+q}{2}}\frac{1+(\frac{\nu}{r-2k+2})^2}{r-2k+1} \tag{3.21}$$

and $\mu_{-1}^{p,q}=0$. Note that $\mu_1^{p,q}$ does not vanish in general, instead it is given by a lengthy expression. However, it turns out that this expression is identically obtained from the recursion for $n=1$ when setting $\mu_0^{p,q}$ to the value above and formally setting $\mu_{-1}^{p,q}=0$. Setting $p=q=0$ this recursion is identical to (3.5), except that r is defined differently in the 3D case.

3.2.3 Second to fourth moment

The second moment, that is, the variance matrix, is given by

$$M_{ij} = A_{ik}A_{jl}\iiint_{\mathbb{R}^3}(\tilde{c}_k-\tilde{v}_k)(\tilde{c}_l-\tilde{v}_l) f^{(\mathrm{P3})}d\tilde{\mathbf{c}}, \tag{3.22}$$

where we have from tensor representation theory

$$\tilde{M}_{kl} = \iiint_{\mathbb{R}^3}(\tilde{c}_k-\tilde{v}_k)(\tilde{c}_l-\tilde{v}_l) f^{(\mathrm{P3})}d\tilde{\mathbf{c}} = \alpha n_k n_l + \beta\delta_{kl}. \tag{3.23}$$

Multiplying by $n_k n_l$ and δ_{kl} yields the equations

$$\tilde{\mu}_2^{0,0} = \alpha + \beta, \qquad \tilde{\mu}_2^{0,0} + \tilde{\mu}_0^{2,0} + \tilde{\mu}_0^{0,2} = \alpha + 3\beta \tag{3.24}$$

for α and β. From the recursion formula we find $\tilde{\mu}_0^{2,0} = \tilde{\mu}_2^{2,0}$ and thus $\alpha = 0$ and $\beta = \tilde{\mu}_2^{0,0}$. Hence, the second moment reads

$$\mathbf{M} = \mathbf{\Theta} = \tilde{\mu}_2^{0,0} \mathbf{A}^2 = \frac{1 + \left(\frac{v}{r}\right)^2}{r-1} \mathbf{A}^2, \tag{3.25}$$

where we introduced the temperature tensor $\mathbf{\Theta}$.

Following the same derivation for the third moment as for the second, we first have the representation

$$\begin{aligned} M_{ijk} &= A_{il} A_{jp} A_{kq} \iiint_{\mathbb{R}^3} (\tilde{c}_l - \tilde{v}_l)(\tilde{c}_p - \tilde{v}_p)(\tilde{c}_q - \tilde{v}_q) f^{(\mathrm{P3})} d\tilde{\mathbf{c}} \\ &= A_{il} A_{jp} A_{kq} \left(\alpha n_l n_p n_q + \beta n_{(l} \delta_{pq)} \right) = A_{il} A_{jp} A_{kq} \tilde{M}_{lpq}. \end{aligned} \tag{3.26}$$

Multiplication of $\tilde{M}_{lpq}$ with $n_l n_p n_q$ and $n_l \delta_{pq}$ gives equations for α and β that involve $\tilde{\mu}_3^{0,0}$, $\tilde{\mu}_1^{2,0}$, and $\tilde{\mu}_1^{0,2}$. We additionally have $\tilde{\mu}_1^{2,0} = \tilde{\mu}_1^{0,2} = \frac{1}{2}\tilde{\mu}_3^{0,0}$ from the recursion formula and with this the solution reads $\alpha = -\frac{1}{2}\tilde{\mu}_3^{0,0}$ and $\beta = \frac{3}{2}\tilde{\mu}_3^{0,0}$. Thus, the third moment is given by

$$M_{ijk} = \tilde{\mu}_3^{0,0} A_{il} A_{jp} A_{kq} \left(-\frac{1}{2} n_l n_p n_q + \frac{3}{2} n_{(l} \delta_{pq)} \right). \tag{3.27}$$

The fourth moment can be represented

$$\begin{aligned} M_{ijkl} &= A_{il} A_{jp} A_{kq} A_{ls} \iiint_{\mathbb{R}^3} (\tilde{c}_l - \tilde{v}_l)(\tilde{c}_p - \tilde{v}_p)(\tilde{c}_q - \tilde{v}_q)(\tilde{c}_s - \tilde{v}_s) f^{(\mathrm{P3})} d\tilde{\mathbf{c}} \\ &= A_{il} A_{jp} A_{kq} A_{ls} \left(\alpha n_l n_p n_q n_s + \beta n_{(l} n_p \delta_{qs)} + \gamma \delta_{(lp} \delta_{qs)} \right) = A_{il} A_{jp} A_{kq} A_{ls} \tilde{M}_{lpqs} \end{aligned} \tag{3.28}$$

and multiplication of $\tilde{M}_{lpqs}$ with $n_l n_p n_q n_s$, $n_l n_p \delta_{qs}$ and $\delta_{lp}\delta_{qs}$ gives equations for α, β, and γ with the solution

$$\alpha = \tilde{\mu}_0^{4,0} - \tilde{\mu}_4^{0,0}, \quad \beta = -2\left(\tilde{\mu}_0^{4,0} - \tilde{\mu}_4^{0,0} \right), \quad \gamma = \tilde{\mu}_0^{4,0}. \tag{3.29}$$

We now introduce the dimensionless quantities

$$\begin{aligned} Q &= \frac{\tilde{\mu}_3^{0,0}}{\left(\tilde{\mu}_2^{0,0}\right)^{3/2}} = \frac{4v}{r-2} \sqrt{\frac{r-1}{r^2+v^2}}, \\ D &= \frac{\tilde{\mu}_4^{0,0}}{\left(\tilde{\mu}_2^{0,0}\right)^2} = \frac{3(r-1)}{(r-2)(r-3)} \left(6 + r - \frac{8r^2}{r^2+v^2} \right), \end{aligned} \tag{3.30}$$

which are analogously defined in the one dimensional case. According to (3.7), the parameters r and ν and thus all $\mu_n^{p,q}$ become functions of Q and D. In particular, we find

$$\tilde{\mu}_0^{4,0} = \left(1 - \frac{3}{4}Q^2/D\right)\tilde{\mu}_4^{0,0}.$$

With the definition

$$\mathbf{N} = \boldsymbol{\Theta}^{1/2}\mathbf{n}, \tag{3.31}$$

we can write the third and fourth moment in the form

$$M_{ijk} = \frac{1}{2}Q\left(-N_iN_jN_k + 3N_{(i}\Theta_{jk)}\right), \tag{3.32}$$

$$M_{ijkl} = \left(D - \frac{3}{4}Q^2\right)\Theta_{(ij}\Theta_{kl)} + \frac{3}{4}Q^2\left(-N_iN_jN_kN_l + 2N_{(i}N_j\Theta_{kl)}\right). \tag{3.33}$$

3.2.4 Reduction to Maxwellian

According to (3.25) we have $\mathbf{A} = \sqrt{(2\bar{m}-5)\boldsymbol{\Theta}}$ for $\nu = 0$ and it can be shown that similar to the one-dimensional case

$$\begin{aligned}\lim_{\bar{m}\to\infty} f^{(\mathrm{P3})}(\mathbf{c};\boldsymbol{\lambda},\mathbf{A},\bar{m},0,\mathbf{n}) &= \lim_{\bar{m}\to\infty} \frac{1}{\det(\mathbf{A})K} \frac{1}{\left(1+(\mathbf{c}-\boldsymbol{\lambda})^T\mathbf{A}^{-2}(\mathbf{c}-\boldsymbol{\lambda})\right)^{\bar{m}}} \\ &= \frac{1}{\sqrt{\det(2\pi\boldsymbol{\Theta})}}\exp\left(-\frac{1}{2}(\mathbf{c}-\boldsymbol{\lambda})^T\boldsymbol{\Theta}^{-1}(\mathbf{c}-\boldsymbol{\lambda})\right).\end{aligned} \tag{3.34}$$

Hence, the Pearson distribution reduces to an anisotropic Gaussian. In that case the shift is nothing but the velocity $\boldsymbol{\lambda} = \mathbf{v}$. If additionally the temperature tensor is isotropic $\boldsymbol{\Theta} = \theta\mathbf{I}$, the distribution function reduces to the Maxwellian (2.8). In the solution of the moment equations this reduction to the Maxwellian distribution is realized by relaxation of the non-equilibrium variables. This relaxation forces the heat flux and thus ν to vanish and the temperature tensor to become isotropic.

4 Moment equations

We will use Pearson-Type-IV distribution functions as distribution model to solve the closure problem in kinetic theory.

4.1 1D: An instructive study

It is instructive to investigate the case of a one-dimensional velocity space for f. The kinetic equation (2.7) then reduces to

$$\partial_t f + c\partial_x f = 0 \tag{4.1}$$

with a real-valued velocity c. We consider the moments up to fourth order

$$\rho = m\int f(c)dc, \quad \rho v = m\int cf(c)dc, \quad \rho\theta = m\int (c-v)^2 f(c)dc, \tag{4.2}$$

$$q = m\int (c-v)^3 f(c)dc, \quad \Delta = m\int (c-v)^4 f(c)dc, \tag{4.3}$$

which are all scalar in this case. They have an interpretation of density ρ, mean velocity v, temperature θ and a quasi-heat flux q. Temperature, heat flux and fourth moment are defined as central or non-convective moments integrating the distribution function shifted by the mean velocity v.

4.1.1 Five moment equations

The corresponding moment equations for the five moments given in (4.2)/(4.3) read

$$\begin{aligned}
&\partial_t\rho + \partial_x\rho v = 0,\\
&\partial_t\rho v + \partial_x\left(\rho v^2 + \rho\theta\right) = 0,\\
&\partial_t\left(\rho v^2 + \rho\theta\right) + \partial_x\left(\rho v^3 + 3\rho\theta v + q\right) = 0,\\
&\partial_t\left(\rho v^3 + 3\rho\theta v + q\right) + \partial_x\left(\rho v^4 + 6\rho\theta v^2 + 4qv + \Delta\right) = 0,\\
&\partial_t\left(\rho v^4 + 6\rho\theta v^2 + 4qv + \Delta\right) + \partial_x\left(\rho v^5 + 10\rho\theta v^3 + 10qv^2 + 5\Delta v^2 + R\right) = 0,
\end{aligned} \tag{4.4}$$

with the highest central moment

$$R = m\int (c-v)^5 f(c)dc, \tag{4.5}$$

which needs to be related to the lower moments in order to close the system. It is easy to set up the model distribution of Grad (2.15) specialized to the one-dimensional case with up to fourth order moments given. The result for the fifth moment is

$$R^{(\mathrm{Grad})} = 10\theta q, \tag{4.6}$$

that is, R is proportional to heat flux. Similar to the full 3D case discussed above, the resulting moment equations are not hyperbolic. The region of hyperbolicity can be displayed in the plane spanned by the dimensionless quantities $q/(\rho\theta^{3/2})$ and $\Delta/(\rho\theta^2)$ and is shown on the left hand side of Fig. 3 (green area). Equilibrium is given at the black dot in the middle of the plot. Note, that the even moment Δ exhibits an equilibrium value of $3\rho\theta^2$. The figure also shows the result of a Riemann problem with a density and pressure ratio of 4.5 which reaches into the elliptic region and develops oscillations. The qualitative behavior is identical to the 3D case shown in Fig. 1.

To establish hyperbolicity we suggest to take a Pearson-IV distribution as model. We write

$$f(c) = \frac{\rho}{m} f^{(\mathrm{P1})}\left(c;\lambda,a,1+\tfrac{r}{2},\nu\right), \tag{4.7}$$

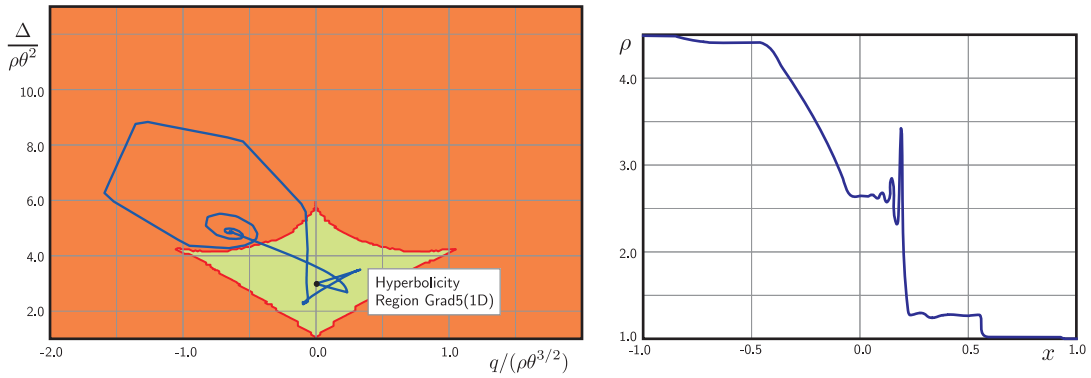

Figure 3: One-dimensional kinetic theory: Failure of Grad closure similar to the full 3D case. The right plot the solution of a Riemann problem. It is also shown in the phase space together with the hyperbolicity region (in green) in the left plot.

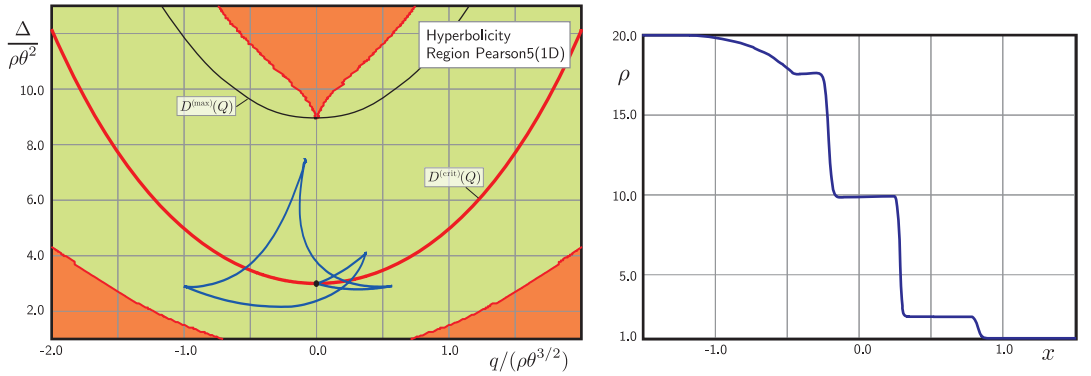

Figure 4: One-dimensional kinetic theory: Left: Hyperbolicity region (green area) with Riemann problem for Pearson5-closure. Right: Riemann problem solution for density.

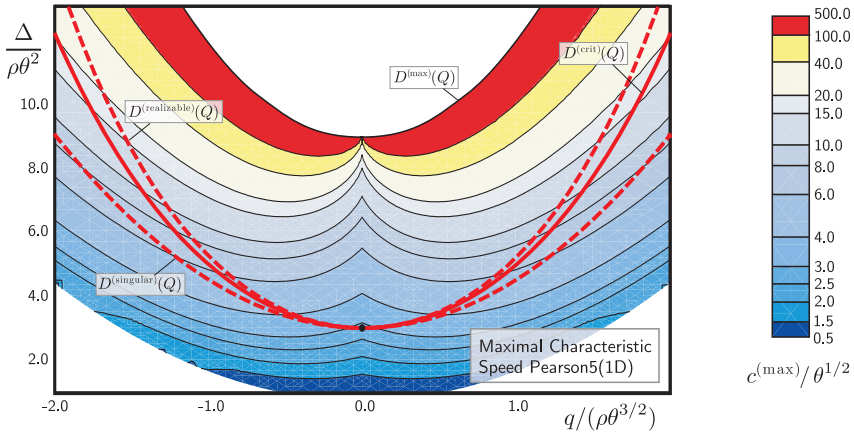

Figure 5: One-dimensional kinetic theory: Contours of maximal characteristic speed of Pearson5 closure.

with $f^{(\mathrm{P1})}$ from (3.1) but we used r from (3.3) as shape parameter, and m as the particle mass. As shown above moments up to fourth order are necessary and sufficient to fix the parameters of the Pearson distribution. The essential parameters from (3.6) are in this context given by

$$Q=\frac{q}{\rho\theta^{3/2}},\quad D=\frac{\Delta}{\rho\theta^2}, \tag{4.8}$$

and with these we can compute the parameters of the distribution via (3.7). The recursion for the moments (3.5) finally gives an explicit expression for the fifth moment

$$R^{(\mathrm{Pearson5})}(Q,D)=2\theta q\frac{D^2-3Q^2+7D}{3Q^2-D+9},\quad D<D^{(\max)}(Q)=9+3Q^2. \tag{4.9}$$

We denote this closure by Pearson5, expressing the fact that we used 5 moment equations in (4.4). Note, that when the fraction in (4.9) is expanded around $(Q,D)=(0,3)$, we obtain the result of Grad (4.6). Hence, the Pearson5-closure is a non-linear extension of Grad. For $D=D^{(\max)}(Q)=9+3Q^2$ the fifth moment tends to infinity, because the shape factor r and hence the exponent $\bar{m}$ in (3.1) becomes too small for the fifth moment to exist. Fig. 4 shows the region of hyperbolicity of the Pearson5-closure (green area) together with the solution of a Riemann problem with density and pressure ratio of 20. The result is free of oscillations.

For given third and fourth moment the Pearson distribution is only realizable if $D>D^{(\mathrm{crit})}(Q)$ holds as stated in (3.8). This corresponds to the region above the red line in Fig. 4. Interestingly, hyperbolicity is also given below this line and also the solution of the Riemann problem does not respect this realizability constraint. It seems that the singularity occurring in the expression for ν in (3.7) cancels out in the closure of the moment equations. Indeed, the relation (4.9) does not show any problems along this line. However, the singularity of $R^{(\mathrm{Pearson5})}$ at $D=D^{(\max)}(Q)$ can be observed in the moment equations. This line is given as black line in Fig. 4. To investigate this singularity we plot the hyperbolicity region in Fig. 5 together with contours of the maximal characteristic speed of the system. It is clearly seen that along the line $D=D^{(\max)}(Q)$ the maximal characteristic speed becomes infinite as the result of the singularity of R. The dashed lines in Fig. 5 will be discussed below.

4.1.2 Four moment equations

If we only consider moments up to third order, the relevant moment equations are given by (4.4) with dropping the last line. The basic variables are (ρ,v,θ,q) and Δ requires a closure. This situation corresponds to the 13-moment-equations in 3D.

Grad's distribution function gives $\Delta=3\rho\theta^2$ but again this shows only limited hyperbolicity for $q/(\rho\theta^{3/2})<0.91$. To use Pearson's distribution requires to fix one parameter in the definition (3.1) or equivalently, relate one moment to all the others.

We will use the reduction $D=D(Q)$ by defining an appropriate curve in Fig. 5. Naturally, the curves should contain the equilibrium point $(Q,D)=(0,3)$. The closure then

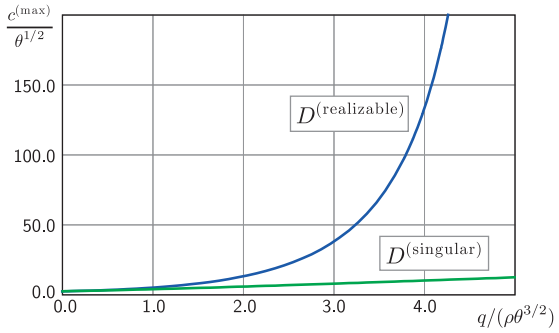

Figure 6: One-dimensional kinetic theory: Maximal characteristic velocities for the reduced moment equations with both realizable and singular Pearson4-closure.

follows from

$$\Delta^{(\text{Pearson4})} = \rho\theta^2 D(q/(\rho\theta^{3/2})). \tag{4.10}$$

Two interesting examples are shown in the figure by dashed lines. The first curve lies in the realizable region and has been obtained from estimating the critical curve (3.8) by

$$D^{(\text{crit})} < \frac{48+39Q^2+3\sqrt{(4+Q^2)^4}}{32-Q^2} = 3\left(1+Q^2\frac{22+Q^2}{32-Q^2}\right), \tag{4.11}$$

which gives

$$D^{(\text{realizable})}(Q) = 3\left(1+Q^2\frac{22+Q^2}{32-Q^2}\right), \quad |Q| < \sqrt{32}. \tag{4.12}$$

With this closure the solution of the reduced moment system with four equations will always have an underlying realizable Pearson Type IV distribution function. For $|Q| \to \sqrt{32}$ the maximal characteristic speed tends to infinity.

The second dashed curve in Fig. 5 represents another interesting case. Along the line

$$D^{(\text{singular})}(Q) = 3\left(1+\frac{1}{2}Q^2\right), \tag{4.13}$$

the shape factor r (and thus m) becomes infinite as can be seen from (3.7). As a result the distribution function shows exponential decay. To some extend this case is closest to the exponential distribution functions of Grad or maximized-entropy-distributions. Even though there exists no realizable Pearson distribution it turns out that the induced moment equations show an extended region of hyperbolicity with no limitation for Q. Additionally, the maximal characteristic speed exhibits smaller values. The situation is depicted in Fig. 6 where the maximal speed is shown for the closure based on $D^{(\text{realizable})}$ and for the closure $D^{(\text{singular})}$. In the first case the speed increases quickly and becomes infinite at $Q = \sqrt{32} \approx 5.66$, while the second curve has much more modest speed values.

4.2 3-D closure

In the full three dimensional case we consider the 13 moments

$$\rho = m\int f(\mathbf{c})\,d\mathbf{c}, \quad \rho v_i = m\int c_i f(\mathbf{c})\,d\mathbf{c}, \quad \frac{3}{2}\rho\theta = m\int \frac{1}{2}\mathbf{C}^2 f(\mathbf{C})\,d\mathbf{C}, \tag{4.14}$$

$$p_{ij} = m\int C_i C_j f(\mathbf{C})\,d\mathbf{C}, \quad q_i = m\int \frac{1}{2}\mathbf{C}^2 C_i f(\mathbf{C})\,d\mathbf{C}, \tag{4.15}$$

that is, density ρ, velocity v_i, temperature θ, pressure tensor p_{ij} and heat flux q_i. The central moments are based on the velocity $C_i = c_i - v_i$. The pressure $p = \rho\theta$ is the trace of the pressure tensor $p_{kk} = 3p$. Dividing the pressure tensor by density yields the temperature tensor such that $p_{ij} = \rho\Theta_{ij}$ and $\theta = 3\Theta_{kk}$. The corresponding moment equations are given by

$$\begin{aligned}
&\frac{\partial}{\partial t}\rho + \frac{\partial}{\partial x_i}(\rho v_i) = 0,\\
&\frac{\partial}{\partial t}(\rho v_i) + \frac{\partial}{\partial x_j}\left(\rho v_i v_j + p_{ij}\right) = 0,\\
&\frac{\partial}{\partial t}\left(\rho v_i v_j + p_{ij}\right) + \frac{\partial}{\partial x_k}\left(\rho v_i v_j v_k + 3p_{(ij}v_{k)} + m_{ijk}\right) = 0,\\
&\frac{\partial}{\partial t}\left(\left(\frac{1}{2}\rho v_k^2 + \frac{3}{2}p\right)v_i + p_{ik}v_k + q_i\right) + \frac{\partial}{\partial x_j}\left(\left(\frac{1}{2}\rho v_k^2 + \frac{3}{2}p\right)v_i v_j + \frac{1}{2}p_{ij}v_k^2\right.\\
&\qquad\qquad \left. + 2v_{(i}p_{j)k}v_k + 2q_{(i}v_{j)} + m_{ijk}v_k + \frac{1}{2}R_{ij}\right) = 0,
\end{aligned} \tag{4.16}$$

which require closures for the higher moments

$$m_{ijk} = m\int C_i C_j C_k f(\mathbf{C})\,d\mathbf{C} \quad \text{and} \quad R_{ij} = m\int C_i C_j \mathbf{C}^2 f(\mathbf{C})\,d\mathbf{C}. \tag{4.17}$$

Note that the trace of the third moment is related to the heat flux $q_i = \frac{1}{2}m_{ikk}$.

For the closure we use the 3D Pearson distribution (3.10) and write

$$f(\mathbf{c}) = \frac{\rho}{m} f^{(\mathrm{P3})}\left(\mathbf{c};\boldsymbol{\lambda},\mathbf{A},2+\tfrac{r}{2},\nu,\mathbf{n}\right) \tag{4.18}$$

as distribution model with r from (3.15). As introduced in Section 3.2.3 we replace the parameters ν and r by Q and D according to (3.30). The parameter Q and the direction $\mathbf{n}$ have to follow from the trace of the general third moment M_{ijk} given in (3.32), which corresponds to the heat flux in our case. We find

$$q_i = \frac{\rho}{2}M_{ikk} = \frac{\rho}{2}Q\left(\frac{1}{2}\left(3\theta - N_k^2\right)\delta_{ik} + \Theta_{ik}\right)N_k \tag{4.19}$$

or using the definition (3.31)

$$q_i = \frac{\rho}{2} Q \Theta_{ij}^{1/2} \left(\frac{1}{2} (3\theta - n_l \Theta_{lm} n_m) \delta_{jk} + \Theta_{jk} \right) n_k, \tag{4.20}$$

where we re-introduced the vector **n** explicitly.

For $i=1,2,3$ these are three equations to compute the direction **n** and Q, since density and temperature tensor are known. The equations are non-linear in the components of n and can not be explicitly solved. However, it is possible to design a simple iteration to find the solution approximately with only few matrix inversions.

Algorithm 4.1:

Let the matrix $B_{ik}(\kappa)$ be defined by

$$B_{ik}(\kappa) = \Theta_{ij}^{1/2} \left(\frac{3\theta - \kappa}{2} \delta_{jk} + \Theta_{jk} \right). \tag{4.21}$$

With $\kappa = \theta$ we find the zeroth iteration $Q^{(0)}$ and $n_i^{(0)}$ for Q and n_i by inversion

$$\tilde{n}_i^{(0)} = \frac{2}{\rho} B_{ik}^{-1}(\theta) q_k, \quad Q^{(0)} = \left\| \tilde{n}_i^{(0)} \right\|, \quad n_i^{(0)} = \frac{\tilde{n}_i^{(0)}}{Q^{(0)}} \tag{4.22}$$

and successive approximations by

$$\tilde{n}_i^{(s)} = \frac{2}{\rho} B_{ik}^{-1} \left(n_l^{(s-1)} \Theta_{lm} n_m^{(s-1)} \right) q_k, \quad Q^{(s)} = \left\| \tilde{n}_i^{(s)} \right\|, \quad n_i^{(s)} = \frac{\tilde{n}_i^{(s)}}{Q^{(s)}} \tag{4.23}$$

for $s=1,2,\cdots$.

Convergence of this fix point iteration can be demonstrating in a straight forward way using the fact that B_{ik} is positive definite for $0<\kappa<3\theta$. Numerical evaluation shows that $s=1$ already gives a very good approximation to the exact solution. The norm of the deviation of the true and approximated direction is below 2%, with the maximum deviation occurring for extreme values of the temperature tensor.

Once Q and n_i are known the full third moment can be evaluated using (3.32) and yields

$$\begin{aligned} m_{ijk}^{(\text{Pearson13})} &= \rho M_{ijk} \\ &= \frac{\rho}{2} Q \left(-N_i N_j N_k + 3 N_{(i} \Theta_{jk)} \right) \end{aligned} \tag{4.24}$$

with $N_i=\Theta_{ij}^{1/2}n_j$. Similarly, the trace of the fourth moment (3.33) is given by

$$\begin{aligned}R_{ij}^{(\text{Pearson13})}&=\rho M_{ijkk}\\&=\rho\left(D-\frac{3}{4}Q^2\right)\left(\Theta_{ij}\theta+\frac{2}{3}\Theta_{ij}^2\right)\\&\quad+\rho\frac{Q^2}{4}\left(3\left(\theta-\mathbf{N}^2\right)N_iN_j+\mathbf{N}^2\Theta_{ij}+4N_k\Theta_{k(i}N_{j)}\right),\end{aligned}\tag{4.25}$$

which requires the knowledge of D. At this point we use the reduced Pearson4-closures of the one-dimensional setting above. Hence, the two possibilities $D=D^{(\text{realizable})}(Q)$ or $D=D^{(\text{singular})}(Q)$ given in (4.12) and (4.13) will be investigated.

4.3 3-D closure in one space dimension

In order to study hyperbolicity of the new closure we specialize the equation to processes that vary only in a single space dimension. The 13 fields reduce to five relevant variables

$$U=\{\rho,v_x,p,p_{xx},q_x\}\tag{4.26}$$

with the equations

$$\begin{aligned}&\partial_t\rho+\partial_x\rho v_x=0,\\&\partial_t\rho v_x+\partial_x\left(\rho v_x^2+p_{xx}\right)=0,\\&\partial_t\left(\frac{1}{2}\rho v_x^2+\frac{3}{2}p\right)+\partial_x\left(\left(\frac{1}{2}\rho v_x^2+\frac{3}{2}p\right)v_x+p_{xx}v_x+q_x\right)=0,\\&\partial_t\left(\rho v_x^2+p_{xx}\right)+\partial_x\left(\rho v_x^3+3p_{xx}v_x+m_{xxx}\right)=0,\\&\partial_t\left(\left(\frac{1}{2}\rho v_x^2+\frac{3}{2}p\right)v_x+p_{xx}v_x+q_x\right)+\partial_x\left(\left(\frac{1}{2}\rho v_x^2+\frac{3}{2}p\right)v_x^2+\frac{5}{2}p_{xx}v_x^2\right.\\&\qquad\left.+2q_xv_x+m_{xxx}v_x+\frac{1}{2}R_{xx}\right)=0,\end{aligned}\tag{4.27}$$

where m_{xxx} and R_{xx} require closure relations. In one space dimensional processes the pressure tensor is diagonal and can be written $p_{ij}=\text{diag}(p+\sigma,p-\frac{1}{2}\sigma,p-\frac{1}{2}\sigma)$ using the shear stress $\sigma=p_{xx}-p=\rho(\Theta_{xx}-\theta)$. With this we have $\Theta_{xx}/\theta=1+\sigma/p$. Additionally, we have $q_i=(q_x,0,0)$ which together with the structure of p_{ij} induces $n_i=(1,0,0)$ and $N_i=(\sqrt{\Theta_{xx}},0,0)$. Hence, the equation (4.19) for Q can be written

$$q_x=\frac{\rho}{2}Q\left(\frac{3}{2}\theta+\frac{1}{2}\Theta_{xx}\right)\sqrt{\Theta_{xx}}\tag{4.28}$$

and we find

$$Q=\frac{4q_x}{\rho\theta\sqrt{\Theta_{xx}}(3+\Theta_{xx}/\theta)}=\frac{q_x}{\rho\theta^{3/2}\sqrt{1+\sigma/p}\,(1+\frac{1}{4}\sigma/p)}\tag{4.29}$$

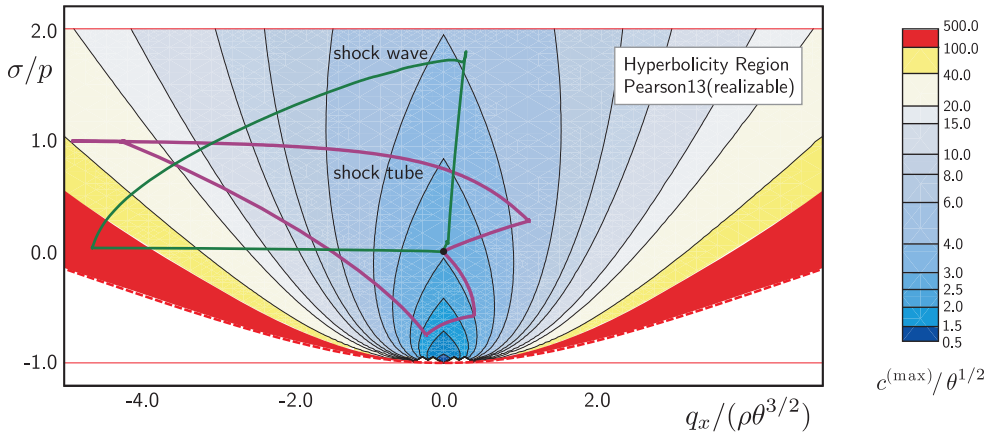

Figure 7: Realizable Pearson closure for 3D moment equations. The figure shows the hyperbolicity region with contours of the maximal characteristic speed in one space dimension. Additionally, pathes of shock tube and shock wave Riemann problems are displayed according to Section 6.

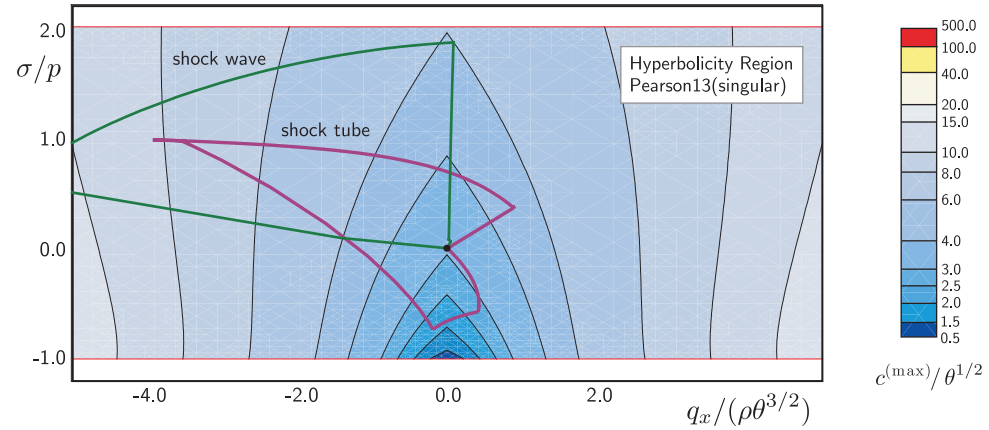

Figure 8: Singular Pearson closure for 3D moment equations. The figure shows the hyperbolicity region with contours of the maximal characteristic speed in one space dimension. Additionally, pathes of shock tube and shock wave Riemann problems are displayed according to Section 6.

as explicit expression for Q. For the closure for m_{xxx} and R_{xx} we now easily find with (4.24) and (4.25) the relations

$$m_{xxx}^{(\text{Pearson13})} = q_x \frac{1+\sigma/p}{1+\frac{1}{4}\sigma/p} \quad \text{and} \quad R_{xx}^{(\text{Pearson13})} = \frac{\rho D\theta^2}{3}(1+\sigma/p)(5+2\sigma/p), \tag{4.30}$$

where we have to use $D = D^{(\text{realizable})}(Q)$ or $D = D^{(\text{singular})}(Q)$ as given in (4.12) and (4.13).

The hyperbolicity region for both cases are shown in Fig. 7 and Fig. 8 together with contours of maximal characteristic speeds. Both figures can be compared to the hyperbolicity region of Grad's 13-moment-equations shown in Fig. 1. The first figure shows the realizable closure for which the fourth moment R_{xx} becomes infinite when $|Q| \to 32$.

This defines a line in the plane of Fig. 7 towards which the maximal characteristic speed also tends to infinity. Apart from this the equations stay hyperbolic for physical values of $\sigma/p<2$.

The singular closure shown in Fig. 8 does not show any tendency for infinite maximal characteristic speed. From the contours it is visible that close to equilibrium in the origin both closures are equivalent. However, the singular closures shows a much more moderate growth of the maximal speed. Hence, even though it lacks an underlying explicitly realizable distribution function this closure might be of better use in numerical computations. Numerical examples considering Riemann problems for both Pearson13-closures are presented below.

5 Discussion

The proposed closures can be discussed from different point of views.

5.1 Numerical point of view

The approximation of the kinetic equation (2.7) by moments can be viewed as a type of spectral method using monomials as test functions and an ansatz space represented by the model for the distribution function. Numerically, the obvious choice for the ansatz space would be the linear space opened by compact basis function, for example hat functions $\varphi_i(\mathbf{c})$. The distribution would have the form $f(\mathbf{c})=\sum\lambda_i\varphi_i(\mathbf{c})$. The resulting system of moment equations would be strongly related to standard discrete velocity schemes for kinetic equations. Even though such an approach is very simple, the clear disadvantages are that the Maxwell distribution, i.e., equilibrium, can not be exactly represented with this ansatz and the moment equations also do not exhibit Galilei invariance. Furthermore, positivity of the distribution function is not easily assured. Interestingly, hyperbolicity of discrete velocity schemes is obvious, because every value of the distribution function is simply advected.

The Pearson distribution (3.10) must be viewed as a representation of a non-linear ansatz space that includes Maxwell distribution and guarantees Galilei invariance and positivity. There is no general theory that gives statements about hyperbolicity of the resulting moment equations, except for the maximum entropy distribution (2.16). Hence, hyperbolicity can only be checked numerically as done in this paper.

The singular closure seems to exhibit a global region of hyperbolicity for all physical values of the phase space. However, the corresponding distribution function is not realizable. As alternative, the realizable closure shows loss of hyperbolicity for some physical values of the phase space. However, this loss of hyperbolicity can be considered robust because of the following reason. In a numerical computation which reaches values close to the border of the hyperbolicity region the characteristic speed tends to infinity forcing the time step of the computation to go to zero before leaving the hyperbolicity region. This behavior simply indicates that the solution shows a non-equilibrium that can not

be represented by a Pearson distribution. Note, that the loss of hyperbolicity in Grad's equations is not robust, i.e., complex eigenvalues arise at finite characteristic speeds.

5.2 Thermodynamical point of view

There is no rigorous a priori statement about the shape of the distribution function except in equilibrium where it becomes a Maxwellian. In this way both the ansatz of Grad (2.15) and the maximum entropy distribution (2.16) are somewhat arbitrary. These ansatzes can be supported by mathematical statements, like a Hermite expansion or entropy maximization, but remain ad hoc. Of course, the choice of a Pearson distribution is no exception. But it leads to practical moment equations contrary to the maximum entropy distribution, and to hyperbolicity in opposition to Grad's equation.

When using the realizable closure (4.12) in (4.25) it is possible to define an entropy from the distribution function (4.18) by

$$\begin{aligned}\eta^{(\mathrm{P3})} &= m\int_{\mathbb{R}^3} f(\mathbf{c})\ln f(\mathbf{c})\,d\mathbf{c}\\ &= -\rho\ln\left(\det(\mathbf{A})K/\rho\right)\\ &\quad -\rho\nu\int_{\mathbb{R}^3}\arctan\left(\mathbf{n}^T\mathbf{A}^{-1}(\mathbf{c}-\boldsymbol{\lambda})\right)f^{(\mathrm{P3})}(\mathbf{c})\,d\mathbf{c}\\ &\quad -\rho\tfrac{r+4}{2}\int_{\mathbb{R}^3}\ln\left(1+(\mathbf{c}-\boldsymbol{\lambda})^T\mathbf{A}^{-2}(\mathbf{c}-\boldsymbol{\lambda})\right)f^{(\mathrm{P3})}(\mathbf{c})\,d\mathbf{c},\end{aligned}\tag{5.1}$$

which reduces to the entropy $\ln\left(p/\rho^{5/3}\right)$ in equilibrium because the Pearson distribution reduces to a Maxwellian in that case. An entropy can not be defined for Grad's distribution due to negative values of the distribution functions. Only in the linearized case Grad's equations can be shown to admit a quadratic entropy, see for example [27]. By definition the maximum entropy distribution allows to write down an entropy which additionally can be shown to be convex. This immediately implies symmetrizing variables for the moment equations and thus hyperbolicity [18]. Convexity for the Pearson entropy (5.1) is unclear and remains future work.

5.3 CFD point of view

Moment equations have been utilized in computational fluid dynamics both for continuum and non-equilibrium flows [16,23,29]. In the case of continuum flows the computational advantage of moment equations over standard compressible viscous flow models is the first order structure which allows numerical methods to use less structured grids. However, especially for high-speed applications the lack of hyperbolicity induced serious drawbacks whenever strong non-equilibrium occurs either local in time or in space. For this reason only the globally hyperbolic 10-moment-equations based on the maximum entropy distribution (2.16) have been used in [16,23].

However, the 10-moment-system assumes vanishing heat conduction which is inappropriate in most high speed flow situations. The proposed closure of this paper based on Pearson distribution offers an alternative which exhibits the necessary robustness due to hyperbolicity and includes heat conduction. If we are only interested in hyperbolic first order equations that model heat conduction and viscous stresses, and not in the detailed approximation of a kinetic equations, the singular closure should be used.

6 Numerical examples

In this section we present some numerical results for (4.27) with the Pearson13 closure in one space dimension. We consider Riemann problems with initial conditions

$$u_0(x) = \begin{cases} (\rho, v_x, p, \sigma, q_x) = (\rho^{(1)}, v_x^{(1)}, p^{(1)}, 0, 0), & x < 0, \\ (\rho, v_x, p, \sigma, q_x) = (\rho^{(0)}, v_x^{(0)}, p^{(0)}, 0, 0), & x \geq 0, \end{cases} \tag{6.1}$$

which develop a series of waves propagating away from the origin. The moment equations are solved with a standard second order finite volume method using a HLL Riemann solver for intercell fluxes and vanLeer-Limiter, see [14].

6.1 Shock tube

The Riemann problem corresponds to a shock tube experiment if we set $v_x^{(0)} = v_x^{(1)} = 0$, $\rho^{(0)} = p^{(0)} = 1$ and $\rho^{(1)} > \rho^{(0)}$, $p^{(1)} > p^{(0)}$. This is both a standard test problem in gas dynamics and for computational methods [14]. In gas dynamics described by Euler equations the result shows a shock wave moving into the low pressure region and a rarefaction fan opening towards the high pressure. The result for the moment equations differ from this picture because we approximate free flight of particles according to (2.7) without any collisions. Only when adding dissipation, like collisional relaxation, to the moment equations the results will turn into the gas dynamical solutions [2,28]. Here, we use these Riemann problems to check and verify the findings about hyperbolicity and study the behavior of the new closure.

First, we choose $\rho^{(1)} = p^{(1)} = 4$ in order to be able to compare to the result of Grad which is shown in the top row of Fig. 1. Due to a different closure by Pearson the wave structure changes as can be seen in Fig. 9, which shows density and heat flux profiles. The similarities of the curves in the plots support the statement given above that Pearson and Grad become equivalent close to equilibrium. Additionally, the realizable and singular closure does not show strong differences.

For large values of $\rho^{(1)}/\rho^{(0)}$ and $p^{(1)}/p^{(0)}$ the Grad closure fails due to lack of hyperbolicity. However, the Pearson closure is capable to compute very strong shock tubes. In Fig. 10 we show the solution for $\rho^{(1)} = p^{(1)} = 50$. The plots show the density, pressure, stress and heat flux profiles both for the realizable and singular closure. Differences are only visible for the first two waves to the right which are faster for the realizable closure.

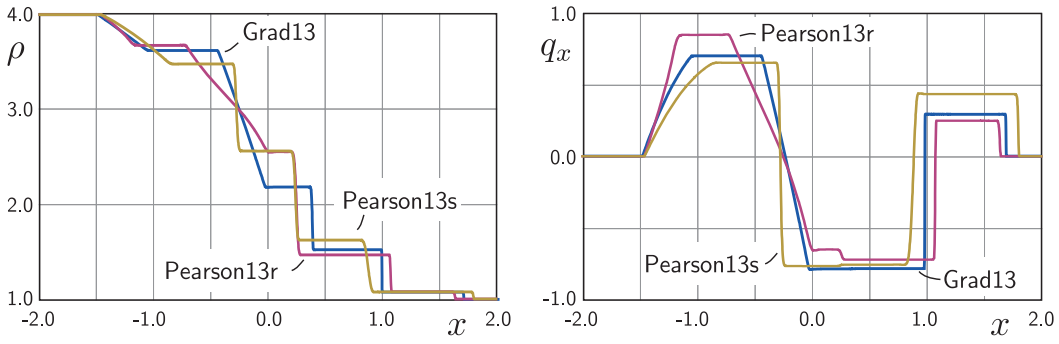

Figure 9: Comparison of the results of Grad13 and Pearson13 closure for a weak shock tube.

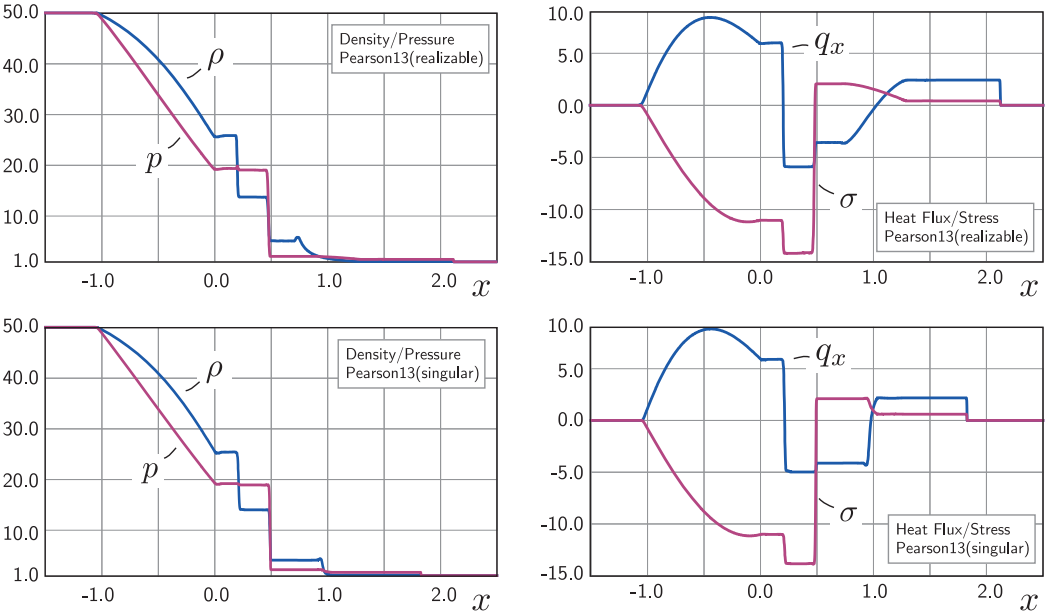

Figure 10: Strong shock tube problem for Pearson13 with realizable and singular closure. Only the first and second wave to the right show significant differences.

The spatial resolution of the numerical method was $\Delta x = 1.3\times10^{-3}$ and the end time $t_{\text{end}} = 0.7$. To satisfy the CFL condition, the constant time step was chosen according to the highest characteristic velocity observed in the solution, which was $c_{\max}/\sqrt{\theta} = 30$ for the realizable and $c_{\max}/\sqrt{\theta} = 5$ for the singular closure. Hence, the computation of the singular closure in Fig. 10 was able to use a clearly bigger time step. Both solutions are shown projected into the region of hyperbolicity in Fig. 7 for the realizable closure and Fig. 8 for the singular closure. From these plots the maximal characteristic speeds can be read off.

Note, that the heat flux and normal stress show very large values in Fig. 10 indicating a very strong non-equilibrium. As soon as dissipation is added to the moment system,

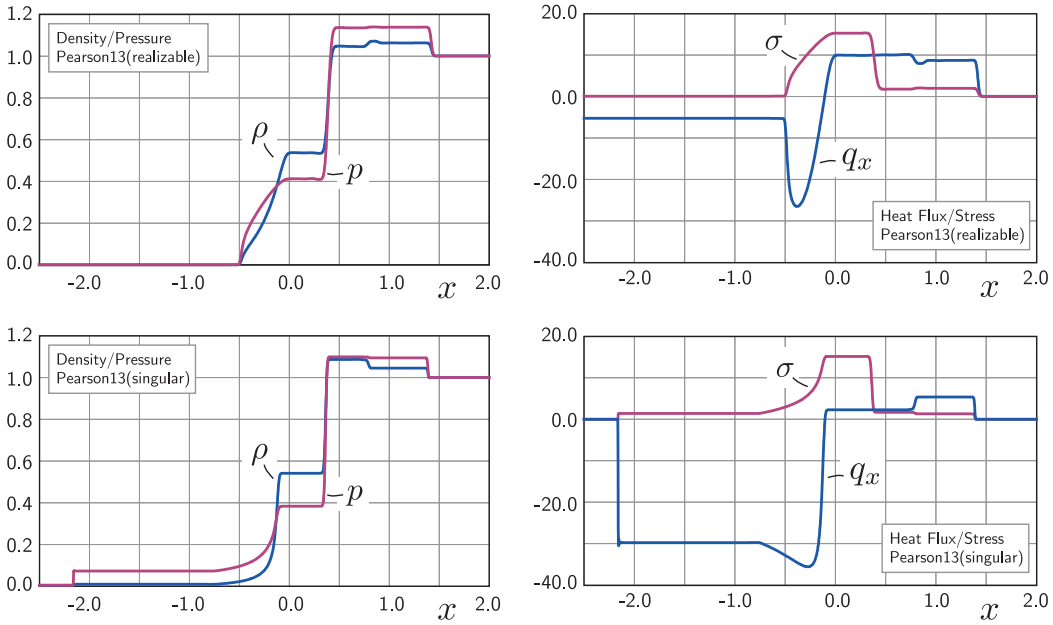

Figure 11: Riemann problem with shock wave initialization for Pearson13 with realizable and singular closure. Significant differences can be observed.

i.e., collisions are included, these values will be damped and decrease quickly with time. The collisionless situation shown here represents the worst case scenario moment equations have to be able to face.

6.2 Shock wave

In another Riemann problem we consider initial data that are chosen from Rankine-Hugoniot conditions connecting a shock wave in classical gas dynamics. That is, we take for the left hand side $(\rho^{(1)},v^{(1)},p^{(1)})=(1,M_0,1)$ with inflow Mach number M_0 and for the right hand side $(\rho^{(0)},v^{(0)},p^{(0)})=(\rho^{(RH)}(M_0),\, v^{(RH)}(M_0),\, p^{(RH)}(M_0))$, see, e.g., [33]. Clearly, the solution of the homogeneous moment equations will not show a shock wave profile due to lack of collisions. Instead, several waves arise similar to the shock tube. When adding dissipation these waves are damped away to create a shock profile. As above, the collisionless setting creates a strong non-equilibrium which represents the worst case situation for moment equations.

Fig. 11 shows the result for $M_0=4$ both for the realizable and singular Pearson13 closure. The values of density and pressure are normalized and shifted such that left and right values are 0 and 1. Both cases use a spatial resolution of $\Delta x=2.25\times10^{-3}$ and the end time $t_{\text{end}}=0.2$. The constant time step was chosen according to the highest characteristic velocity observed in the solution, which was $c_{\max}/\sqrt{\theta}=280$ for the realizable and $c_{\max}/\sqrt{\theta}=15$ for the singular closure.

A close inspection of the result shows that the fastest wave to the left shows significant differences between the closures. For the singular closure, the fastest wave to the left is located at $x=-2.2$ and clearly visible in pressure, stress and heat flux. For the realizable closure this wave is almost not visible in density, pressure, stress and velocity (not shown), but only in heat flux. However, this wave is so fast that for the time shown it has left the domain shown in Fig. 11 (top right) and is located at approximately $x=-9.5$. Viewing the solution in the region of hyperbolicity, Fig. 7 shows that this wave reaches values close to the border and, thus, produces large wave speeds. The solution of the singular closure remains in regions with moderate wave speeds, see Fig. 8.

7 Conclusion

This paper proposes a new practical closure for moment equations in kinetic gas theory that establishes global hyperbolicity. This closure is considerably superior to both the classical Grad closure which is known to have a finite region of hyperbolicity, and the maximum entropy closure which has practical and theoretical problems to produce explicit constitutive relations. As a model for the distribution function the new closure assumes a Pearson-Type-IV distribution which possesses enough parameters to close the moment equations with the 13 fields density, velocity, temperature, pressure deviator and heat flux. A major advantage of the Pearson distribution is that all moments can be expressed analytically. The final closure comes in two variants. The realizable version guarantees the existence of a distribution function for the solution of the moment system, but characteristic speeds may tend to infinity. This is avoided in the singular variant, which however, does not have a realizable distribution function everywhere.

A few solutions of Riemann problems in one space dimension demonstrate the behavior of the closure variants. In future work the new equations have to be studied in one and more dimensions and coupled to dissipation like relaxation and diffusion.

Appendix

A.1 One-dimensional

A.1.1 Velocity

For the velocity of the distribution we again use the transformation $\tilde{c}=(c-\lambda)/a \Leftrightarrow c=a\tilde{c}+\lambda$ to find

$$v=\frac{1}{ak}\int_{-\infty}^{\infty} c\frac{\exp\left(-\nu\arctan\left(\frac{c-\lambda}{a}\right)\right)}{\left(1+\left(\frac{c-\lambda}{a}\right)^2\right)^m}dc=\lambda+\frac{a}{k}\int_{-\infty}^{\infty}\tilde{c}\frac{\exp\left(-\nu\arctan\left(\tilde{c}\right)\right)}{\left(1+\tilde{c}^2\right)^m}d\tilde{c}, \tag{A.1}$$

where the integral can be reduced by the transformation

$$x=\arctan(\tilde{c}) \quad\Leftrightarrow\quad \tilde{c}=\tan x \quad\text{with}\quad dx=\frac{1}{1+\tilde{c}^2}d\tilde{c}=\cos^2 x\, d\tilde{c}. \tag{A.2}$$

This leads to the integral

$$v=\lambda+\frac{a}{k}\int_{-\pi}^{\pi}\sin x\cos^{2(m-1)-1}x\exp(-\nu x)\,dx \tag{A.3}$$

which has the form $\int u(x)v'(x)dx$ and we use partial integration with $v'(x)=\sin x\cos^{2(m-1)-1}x$ and $u(x)=\exp(-\nu x)$ to find

$$v=\lambda-\frac{\nu}{2(m-1)}\frac{a}{k}\int_{-\infty}^{\infty}\cos^{2(m-1)}x\exp(-\nu x)\,dx=\lambda-\frac{a\nu}{2(m-1)} \tag{A.4}$$

after back-transforming of the integral and realizing that f_{P1} is normalized.

A.1.2 Recursion formula

The recursion formula is derived in four steps. First the integral is transformed to a trigonometric integral where then suitable partial integration can be employed. The remaining integrals are then back-transformed and the definition of the moments is used. At last the definition of velocity is inserted. We start with transforming the integral and find

$$\begin{aligned}\mu_n&=\frac{a^n}{k}\int_{-\infty}^{\infty}(\tilde{c}-\tilde{v})^n\frac{\exp(-\nu\arctan(\tilde{c}))}{(1+\tilde{c}^2)^m}d\tilde{c}\\&=\frac{a^n}{k}\int_{-\infty}^{\infty}\tilde{c}(\tilde{c}-\tilde{v})^{n-1}\frac{\exp(-\nu\arctan(\tilde{c}))}{(1+\tilde{c}^2)^m}d\tilde{c}-\tilde{v}a\mu_{n-1},\end{aligned} \tag{A.5}$$

where we introduced the reduced velocity

$$\tilde{v}=-\frac{\nu}{2(m-1)}. \tag{A.6}$$

The integral is now further transformed using the relation (A.2) which gives

$$\mu_n=\frac{a^n}{k}\int_{-\pi}^{\pi}\sin x\cos^{r-n}x(\sin x-\tilde{v}\cos x)^{n-1}\exp(-\nu x)\,dx-\tilde{v}a\mu_{n-1}, \tag{A.7}$$

with $r=2(m-1)$. Here, partial integrations of the form $\int u(x)v'(x)dx$ can be employed with $v'(x)=\sin x\cos^{r-n}x$ and $u(x)=(\sin x-\tilde{v}\cos x)^{n-1}\exp(-\nu x)$ which yields

$$\begin{aligned}\mu_n=\frac{a^n}{r-n+1}\Bigg(&\frac{n-1}{k}\int_{-\pi}^{\pi}\cos^{r-n+1}(x)(\cos x+\tilde{v}\sin x)(\sin x-\tilde{v}\cos x)^{n-2}\exp(-\nu x)dx\\&-\frac{\nu}{a^{n-1}}\mu_{n-1}\Bigg)-\tilde{v}a\mu_{n-1},\end{aligned} \tag{A.8}$$

where the one part of the partial integration result have been identified immediately by μ_{n-1} after back-transforming. The remaining integral is further reduced such that

moments μ_{n-1} and μ_{n-2} can be identified and gives us

$$\begin{aligned}
&\frac{1}{k}\int_{-\pi}^{\pi}\cos^{r-n+1}x(\cos x+\tilde{v}\sin x)(\sin x-\tilde{v}\cos x)^{n-2}\exp(-\nu x)\,dx\\
=&\frac{1}{k}\int_{-\pi}^{\pi}\cos^{r-n+2}x(\sin x-\tilde{v}\cos x)^{n-2}\exp(-\nu x)\,dx\\
&+\tilde{v}\frac{1}{k}\int_{-\pi}^{\pi}\cos^{r-n+1}x\sin x(\sin x-\tilde{v}\cos x)^{n-2}\exp(-\nu x)\,dx\\
=&\frac{1}{a^{n-2}}\mu_{n-2}+\tilde{v}\frac{1}{k}\int_{-\infty}^{\infty}\tilde{c}(\tilde{c}-\tilde{v})^{n-2}\frac{\exp(-\nu\arctan(\tilde{c}))}{(1+\tilde{c}^2)^m}d\tilde{c}\\
=&\frac{1}{a^{n-2}}\mu_{n-2}+\frac{\tilde{v}}{a^{n-1}}\mu_{n-1}+\frac{\tilde{v}^2}{a^{n-2}}\mu_{n-2},
\end{aligned}\tag{A.9}$$

which together with the above leads to

$$\mu_n=\frac{a^n}{r-n+1}\left((n-1)\left(\frac{1}{a^{n-2}}\mu_{n-2}+\frac{\tilde{v}}{a^{n-1}}\mu_{n-1}+\frac{\tilde{v}^2}{a^{n-2}}\mu_{n-2}\right)-\frac{\nu}{a^{n-1}}\mu_{n-1}\right)-\tilde{v}a\mu_{n-1}.\tag{A.10}$$

Finally, this is inserted above together with the definition of the velocity $\tilde{v}$. After some algebra we find

$$\mu_n=\frac{a(n-1)}{r-n+1}\left((1+\left(\frac{\nu}{r}\right)^2)a\mu_{n-2}-2\frac{\nu}{r}\mu_{n-1}\right)\tag{A.11}$$

which is the asserted recursion formula.

A.2 Three-dimensional

A.2.1 Normalization constant and velocity

The normalization constant (3.11) only depends on m and ν which can be seen using the transformation $\tilde{\mathbf{c}}=\mathbf{A}^{-1}(\mathbf{c}-\boldsymbol{\lambda})\Leftrightarrow\mathbf{c}=\mathbf{A}\tilde{\mathbf{c}}+\boldsymbol{\lambda}$ on the integral to produce

$$K(m,\nu)=\iiint_{\mathbb{R}^3}\frac{\exp\left(-\nu\arctan\left(\mathbf{n}^T\tilde{\mathbf{c}}\right)\right)}{\left(1+\tilde{\mathbf{c}}^T\tilde{\mathbf{c}}\right)^m}d\tilde{\mathbf{c}}.\tag{A.12}$$

This integral factorizes in a special way. We choose the coordinate system such that $\tilde{c}_1=\mathbf{n}^T\tilde{\mathbf{c}}$ and $\tilde{\mathbf{c}}^T\tilde{\mathbf{c}}=\tilde{c}_1^2+\tilde{c}_2^2+\tilde{c}_3^2$ with $\tilde{c}_{2,3}=\hat{\mathbf{n}}_{2,3}^T\tilde{\mathbf{c}}$ where $\hat{\mathbf{n}}_{2,3}^T\mathbf{n}=0$ and use the transformations

$$\hat{c}_3=\frac{\tilde{c}_3}{\sqrt{1+\tilde{c}_1^2+\tilde{c}_2^2}},\quad \hat{c}_2=\frac{\tilde{c}_2}{\sqrt{1+\tilde{c}_1^2}},\quad \hat{c}_1=\tilde{c}_1\tag{A.13}$$

successively which leads to

$$\begin{aligned}
K(m,\nu) &= \iiint_{\mathbb{R}^3} \frac{\exp(-\nu\arctan(\tilde{c}_1))}{\left(1+\tilde{c}_1^2+\tilde{c}_2^2+\tilde{c}_3^2\right)^m} d\tilde{\mathbf{c}} \\
&= \int_{\mathbb{R}} \exp(-\nu\arctan(\tilde{c}_1)) \int_{\mathbb{R}} \frac{1}{\left(1+\tilde{c}_1^2+\tilde{c}_2^2\right)^m} \int_{\mathbb{R}} \frac{1}{\left(1+(\frac{\tilde{c}_3}{\sqrt{1+\tilde{c}_1^2+\tilde{c}_2^2}})^2\right)^m} d\tilde{c}_3 d\tilde{c}_2 d\tilde{c}_1 \\
&= \int_{\mathbb{R}} \frac{\exp(-\nu\arctan(\tilde{c}_1))}{\left(1+\tilde{c}_1^2\right)^{m-1/2}} \int_{\mathbb{R}} \frac{1}{\left(1+(\frac{\tilde{c}_2}{1+\tilde{c}_1^2})^2\right)^{m-1/2}} d\tilde{c}_2 d\tilde{c}_1 \int_{\mathbb{R}} \frac{1}{\left(1+\hat{c}_3^2\right)^m} d\hat{c}_3 \\
&= \int_{\mathbb{R}} \frac{\exp(-\nu\arctan(\hat{c}_1))}{\left(1+\hat{c}_1^2\right)^{m-1}} d\hat{c}_1 \int_{\mathbb{R}} \frac{1}{\left(1+\hat{c}_2^2\right)^{m-1/2}} d\hat{c}_2 \int_{\mathbb{R}} \frac{1}{\left(1+\hat{c}_3^2\right)^m} d\hat{c}_3 \\
&= K_1(m,\nu) K_2(m) K_3(m),
\end{aligned} \tag{A.14}$$

where the three constants $K_{1,2,3}$ are given by the three one-dimensional integrals over $\hat{c}_{1,2,3}$, which are nothing but integrals of one-dimensional Pearson distributions. Note that in comparison to the one-dimensional case $K_1(m,\nu)=k(m-1,\nu)$, $K_2(m)=k(m-1/2,0)$ and $K_3(m)=k(m,0)$.

To compute the velocity we need to find α according to (3.13). The integral can be factorized as above and then easily gives

$$\begin{aligned}
\alpha &= \frac{1}{K} \iiint_{\mathbb{R}^3} \mathbf{n}^T \tilde{\mathbf{c}} f^{(\mathrm{P3})}(\tilde{\mathbf{c}};\mathbf{0},\mathbf{I},m,\nu,\mathbf{n}) d\tilde{\mathbf{c}} \\
&= \frac{1}{K_1 K_2 K_3} \int_{\mathbb{R}} \tilde{c}_1 \frac{\exp(-\nu\arctan(\tilde{c}_1))}{\left(1+\tilde{c}_1^2\right)^{m-1}} d\tilde{c}_1 \int_{\mathbb{R}} \frac{1}{\left(1+\hat{c}_2^2\right)^{m-1/2}} d\hat{c}_2 \int_{\mathbb{R}} \frac{1}{\left(1+\hat{c}_3^2\right)^m} d\hat{c}_3 \\
&= -\frac{\nu}{2(m-2)}.
\end{aligned} \tag{A.15}$$

A.2.2 Recursion formula

For the recursion formula we use the same factorization procedure to find

$$\begin{aligned}
\tilde{\mu}_n^{p,q} &= \frac{1}{K} \iiint_{\mathbb{R}^3} (\tilde{c}_1-\tilde{v}_1)^n \tilde{c}_2^p \tilde{c}_3^q \frac{\exp(-\nu\arctan(\tilde{c}_1))}{\left(1+\tilde{c}_1^2+\tilde{c}_2^2+\tilde{c}_3^2\right)^m} d\tilde{\mathbf{c}} \\
&= \frac{1}{K} \int_{\mathbb{R}} (\tilde{c}_1-\tilde{v}_1)^n \frac{\exp(-\nu\arctan(\hat{c}_1))}{\left(1+\hat{c}_1^2\right)^{m-1-\frac{p+q}{2}}} d\hat{c}_1 \int_{\mathbb{R}} \frac{\hat{c}_2^p}{\left(1+\hat{c}_2^2\right)^{m-\frac{q+1}{2}}} d\hat{c}_2 \int_{\mathbb{R}} \frac{\hat{c}_3^q}{\left(1+\hat{c}_3^2\right)^m} d\hat{c}_3.
\end{aligned} \tag{A.16}$$

For the first integral the derivation of the recursion in one dimension given in Section A.1.2 can be used. This derivation essentially operates on n such that when identifying the moments $\tilde{\mu}_{n-1}^{p,q}$ and $\tilde{\mu}_{n-2}^{p,q}$ the back-transform is possible. Hence, we can follow an identical derivation of the recursion for the first integral up to (A.10). The only difference

is that $m^{(1D)}$ in (A.10) has to be replaced by $m^{(3D)}-1-\frac{p+q}{2}$, that is, $r^{(1D)}=2(m^{(1D)}-1)$ is replaced by $2(m^{(3D)}-2-\frac{p+q}{2})$ which we write $r^{(3D)}-p-q$.

However, this replacement of r is not applicable in the definition of $\tilde{v}_1$ where we simply replace $r^{(1D)}$ by $r^{(3D)}$. However, inspection of the one-dimensional derivation shows, that the definition of $\tilde{v}$ only enters in the steps after (A.10) which we have to redo for the 3D case. We find

$$\begin{aligned}\tilde{\mu}_n^{p,q} &= \frac{1}{r-p-q-n+1}\left((n-1)\left(\tilde{\mu}_{n-2}^{p,q}+\tilde{v}_1\tilde{\mu}_{n-1}^{p,q}+\tilde{v}_1^2\tilde{\mu}_{n-2}^{p,q}\right)-\nu\tilde{\mu}_{n-1}^{p,q}\right)-\tilde{v}_1\tilde{\mu}_{n-1}^{p,q}\\ &= \frac{1}{r-p-q-n+1}\left((n-1)\left(1+(\frac{\nu}{r})^2\right)\tilde{\mu}_{n-2}^{p,q}-(2(n-1)+p+q)\frac{\nu}{r}\tilde{\mu}_{n-1}^{p,q}\right) \qquad \text{(A.17)}\end{aligned}$$

which is the asserted formula.

A.2.3 Explicit formula for $\tilde{\mu}_0^{p,q}$

For the explicit formula we have the factorization

$$\begin{aligned}\tilde{\mu}_0^{p,q} &= \frac{1}{K}\iiint_{\mathbb{R}^3}\tilde{c}_2^p\tilde{c}_3^q\frac{\exp(-\nu\arctan(\tilde{c}_1))}{\left(1+\tilde{c}_1^2+\tilde{c}_2^2+\tilde{c}_3^2\right)^m}d\tilde{\mathbf{c}}\\ &= \frac{1}{K_1K_2K_3}\int_{\mathbb{R}}\frac{\exp(-\nu\arctan(\tilde{c}_1))}{\left(1+\tilde{c}_1^2\right)^{m-1-\frac{p+q}{2}}}d\tilde{c}_1\int_{\mathbb{R}}\frac{\hat{c}_2^p}{\left(1+\hat{c}_2^2\right)^{m-1/2-q/2}}d\hat{c}_2\int_{\mathbb{R}}\frac{\hat{c}_3^q}{\left(1+\hat{c}_3^2\right)^m}d\hat{c}_3, \qquad \text{(A.18)}\end{aligned}$$

where the first integral does not cancel with the normalization constant because the exponential in the denominator is different. For the same reason 1D recursions on the second and third integrals can not be used easily, because the identification of the $\tilde{\mu}_0^{p,q}$ becomes difficult due to the differences of the exponentials in the integrands and in the normalization constants. For this reason the recursion have to be applied very carefully.

We define

$$I(b,\nu,n) := \int_{\mathbb{R}} c^n\frac{\exp(-\nu\arctan(c))}{\left(1+c^2\right)^b}dc \qquad \text{(A.19)}$$

such that we have

$$K_1 = I(m-1,\nu,0), \quad K_2 = I(m-1/2,0,0), \quad K_3 = I(m,0,0), \qquad \text{(A.20)}$$

and the 1D recursion (3.5) holds for $\mu_n = I(b,\nu,n)/I(b,\nu,0)$. It reads for $\nu=0$

$$\mu_n = \frac{I(b,0,n)}{I(b,0,0)} = \frac{(n-1)}{2(b-1)-(n-1)}\mu_{n-2} = \frac{(n-1)}{2(b-1)-(n-1)}\frac{I(b,0,n-2)}{I(b,0,0)}. \qquad \text{(A.21)}$$

Additionally, we need the relation

$$\frac{I(b,\nu,0)}{I(b+1,\nu,0)} = \frac{2b}{2b-1}\left(1+(\frac{\nu}{2b})^2\right) \qquad \text{(A.22)}$$

which can be found from the explicit expression for the normalization constant [19]

$$I(b,\nu,0)=\frac{\pi\Gamma(2b-1)}{2^{2(b-1)}\Gamma(b-\mathbf{i}\frac{\nu}{2})\Gamma(b+\mathbf{i}\frac{\nu}{2})}. \tag{A.23}$$

Equipped with this we carefully evaluate one recursion step for $\tilde{\mu}_0^{p,q}$

$$\begin{aligned}
\tilde{\mu}_0^{p,q} &= \frac{I(m-1-\frac{p+q}{2},\nu,0)}{I(m-1,\nu,0)}\frac{I(m-\frac{q+1}{2},0,p)}{I(m-\frac{1}{2},0,0)}\frac{I(m,0,q)}{I(m,0,0)} \\
&= \frac{(p-1)}{2((m-\frac{q+1}{2})-1)-(p-1)}\frac{I(m-1-\frac{p+q}{2},\nu,0)}{I(m-1,\nu,0)}\frac{I(m-\frac{q+1}{2},0,p-2)}{I(m-\frac{1}{2},0,0)}\frac{I(m,0,q)}{I(m,0,0)} \\
&= \frac{(p-1)}{2(m-1-\frac{p+q}{2})}\frac{2(m-1-\frac{p+q}{2})}{2(m-1-\frac{p+q}{2})-1}\left(1+\Big(\frac{\nu}{2(m-1-\frac{p+q}{2})}\Big)^2\right) \\
&\quad\times\frac{I(m-1-\frac{(p-2)+q}{2},\nu,0)}{I(m-1,\nu,0)}\frac{I(m-\frac{q+1}{2},0,p-2)}{I(m-\frac{1}{2},0,0)}\frac{I(m,0,q)}{I(m,0,0)} \\
&= \frac{(p-1)}{2(m-1-\frac{p+q}{2})-1}\left(1+\Big(\frac{\nu}{2(m-1-\frac{p+q}{2})}\Big)^2\right)\tilde{\mu}_0^{p-2,q},
\end{aligned} \tag{A.24}$$

and for $\tilde{\mu}_0^{0,q}$ analogously

$$\begin{aligned}
\tilde{\mu}_0^{0,q} &= \frac{I(m-1-\frac{q}{2},\nu,0)}{I(m-1,\nu,0)}\frac{I(m-\frac{q+1}{2},0,0)}{I(m-1/2,0,0)}\frac{I(m,0,q)}{I(m,0,0)} \\
&= \frac{2(m-1-\frac{q}{2})}{2(m-1-\frac{q}{2})-1}\left(1+\Big(\frac{\nu}{2(m-1-\frac{q}{2})}\Big)^2\right)\frac{I(m-1-\frac{q-2}{2},\nu,0)}{I(m-1,\nu,0)}\frac{I(m-\frac{q+1}{2},0,0)}{I(m-1/2,0,0)}\frac{I(m,0,q)}{I(m,0,0)} \\
&= \frac{2(m-\frac{q+1}{2})}{2(m-\frac{q+1}{2})-1}\frac{2(m-1-\frac{q}{2})}{2(m-1-\frac{q}{2})-1}\left(1+\Big(\frac{\nu}{2(m-1-\frac{q}{2})}\Big)^2\right) \\
&\quad\times\frac{I(m-1-\frac{q-2}{2},\nu,0)}{I(m-1,\nu,0)}\frac{I(m-\frac{(q-2)+1}{2},0,0)}{I(m-1/2,0,0)}\frac{I(m,0,q)}{I(m,0,0)} \\
&= \frac{(q-1)}{2(m-1)-(q-1)}\frac{2(m-\frac{q+1}{2})}{2(m-1-\frac{q}{2})-1}\left(1+\Big(\frac{\nu}{2(m-1-\frac{q}{2})}\Big)^2\right) \\
&\quad\times\frac{I(m-1-\frac{q-2}{2},\nu,0)}{I(m-1,\nu,0)}\frac{I(m-\frac{(q-2)+1}{2},0,0)}{I(m-1/2,0,0)}\frac{I(m,0,q-2)}{I(m,0,0)} \\
&= \frac{(q-1)}{2(m-1-\frac{q}{2})-1}\left(1+\Big(\frac{\nu}{2(m-1-\frac{q}{2})}\Big)^2\right)\tilde{\mu}_0^{0,q-2}.
\end{aligned} \tag{A.25}$$

If we replace $m=r/2+2$ in these expressions we find the recursions

$$\tilde{\mu}_0^{p,q} = \frac{(p-1)}{r-p-q+1}\left(1+\left(\frac{\nu}{r-p-q+2}\right)^2\right)\tilde{\mu}_0^{p-2,q}, \tag{A.26}$$

$$\tilde{\mu}_0^{0,q} = \frac{(q-1)}{r-q+1}\left(1+\left(\frac{\nu}{r-q+2}\right)^2\right)\tilde{\mu}_0^{0,q-2}, \tag{A.27}$$

which directly lead to the explicit formula

$$\tilde{\mu}_0^{p,q} = (p-1)!!(q-1)!!\prod_{k=1}^{\frac{p+q}{2}}\frac{1+(\frac{\nu}{r-2k+2})^2}{r-2k+1} \tag{A.28}$$

as given in the main text.

References

[1] J. D. Au, Lösung nichtlinearer Probleme in der Erweiterten Thermodynamik, Dissertation, Technical University of Berlin (2001).

[2] J. D. Au, M. Torrilhon, and W. Weiss, The shock tube study in extended thermodynamics, Phys. Fluids 13(8), (2001) 2423-2432.

[3] A. V. Bobylev, The Chapman-Enskog and Grad methods for solving the Boltzmann equation, Sov. Phys. Dokl. 27, (1982) 29-31.

[4] F. Brini, Hyperbolicity region in extended thermodynamics with 14 moments, Cont. Mech. Thermodyn. 13(1), (2001) 1.

[5] C. Cercignani, The Boltzmann Equation and its Applications, Applied Mathematical Sciences 67, Springer, New York, (1988).

[6] S. Chapman and T. G. Cowling, The Mathematical Theory of Non-Uniform Gases, Cambridge University Press, Cambridge (1970).

[7] A. Frezzotti and L. Gibelli, A moment method for low speed micro-flows, presented at the Workshop on Moment Methods in Kinetic Theory, Zurich, (2008).

[8] H. Grad, On the kinetic theory of rarefied gases, Comm. Pure Appl. Math. 2, (1949) 331.

[9] H. Grad, Principles of the Kinetic Theory of Gases, in Handbuch der Physik, editor S. Flügge, Springer, Berlin (1958), vol. 12.

[10] X.-J. Gu and D. Emerson, A computational strategy for the regularized 13 moment equations with enhanced wall-boundary conditions, J. Comput. Phys. 225 (2007) 263-283.

[11] J. Heinrich, A Guide to the Pearson Type IV Distribution, CDF Internal Note 6820, Collider Detector at Fermilab, `www-cdf.fnal.gov/publications`, (2004).

[12] M. Junk, Domain of definition of Levermore's five-moment system, J. Stat. Phys. 93(5-6), (1998) 1143-1167.

[13] M. Junk and A. Unterreiter, Maximum entropy moment systems and Galilean invariance, Cont. Mech. Thermodyn. 14(6), (2002) 563-576.

[14] R. J. LeVeque, Finite Volume Methods for Hyperbolic Problems, Cambridge University Press, Cambridge (2002).

[15] C. D. Levermore, Moment closure hierarchies for kinetic theories, J. Stat. Phys. 83(5-6), (1996) 1021-1065.

[16] J. G. McDonald and C. P. T. Groth, Extended Fluid-Dynamic Model for Micron-Scale Flows Based on Gaussian Moment Closure, 46th AIAA Aerospace Sciences Meeting, AIAA 2008-691, (2008).
[17] H. M. Mott-Smith, The solution of the Boltzmann equation for a shock wave, Phys. Rev. 82, (1951) 885-892.
[18] I. Müller and T. Ruggeri, Rational Extended Thermodynamics (2nd ed.), Springer Tracts in Natural Philosophy (vol.37), Springer, New York (1998).
[19] Y. Nagahara, The PDF and CF of Pearson type IV distributions and the ML estimation of the parameters, Stat. Prob. Let. 43, (1999) 251.
[20] K. Pearson, Contributions to the mathematical theory of evolution – II. Skew variation in homogeneous material, Phil. Trans. Royal Soc. London A 186, (1895) 343.
[21] K. Pearson, Mathematical contributions to the theory of evolution – X. Supplement to a memoir on skew variation, Phil. Trans. Royal Soc. London A 197, (1901) 443.
[22] K. Pearson, Mathematical contributions to the theory of evolution – XIX. Second supplement to a memoir on skew variation, Phil. Trans. Royal Soc. London A 216, (1916) 429.
[23] Y. Suzuki and B. van Leer, Application of the 10-moment model to MEMS flows, 43rd AIAA Aerospace Sciences Meeting and Exhibit, AIAA Paper 2005-1398, (2005).
[24] H. Struchtrup, Stable transport equations for rarefied gases at high orders in the Knudsen number, Phys. Fluids 16(11), (2004) 3921-3934.
[25] H. Struchtrup, Derivation of 13 moment equations for rarefied gas flow to second order accuracy for arbitrary interaction potentials, Multiscale Model. Simul. 3(1), (2005) 221-243.
[26] H. Struchtrup and M. Torrilhon, Regularization of Grad's 13-moment-equations: Derivation and linear analysis, Phys. Fluids 15/9, (2003) 2668-2680.
[27] H. Struchtrup and M. Torrilhon, H-theorem, regularization, and boundary conditions for linearized 13 moment equations, Phys. Rev. Letters 99, (2007) 014502.
[28] M. Torrilhon, Characteristic waves and dissipation in the 13-moment-case, Cont. Mech. Thermodyn. 12, (2000) 289.
[29] M. Torrilhon, Two-dimensional bulk microflow simulations based on regularized 13-moment-equations, SIAM Multiscale Model. Simul. 5(3), (2006) 695-728.
[30] M. Torrilhon and H. Struchtrup, Regularized 13-moment-equations: Shock structure calculations and comparison to Burnett models, J. Fluid Mech. 513, (2004) 171-198.
[31] M. Torrilhon and H. Struchtrup, Boundary conditions for regularized 13-moment-equations for micro-channel-flows, J. Comput. Phys. 227(3), (2008) 1982-2011.
[32] D. A. Vereshchagin, S. B. Leble, and M. A. Solovchuk, Piecewise continuous distribution function method in the theory of wave disturbances of inhomogeneous gas, Physics Letters A 348(3-6), (2006) 326-334.
[33] W. G. Vincenti and C. H. Kruger Jr., Introduction to Physical Gas Dynamics, Wiley, New York (1965).